

# Multigrade Neural Network Approximation

**Shijun Zhang\***

*Department of Applied Mathematics  
Hong Kong Polytechnic University*

shijun.zhang@polyu.edu.hk

**Zuowei Shen**

*Department of Mathematics  
National University of Singapore*

matzuows@nus.edu.sg

**Yuesheng Xu**

*Department of Mathematics and Statistics  
Old Dominion University*

y1xu@odu.edu

## Abstract

We study multigrade deep learning (MGDL) as a principled framework for structured error refinement in deep neural networks. While the approximation power of neural networks is now relatively well understood, training very deep architectures remains challenging due to highly non-convex and often ill-conditioned optimization landscapes. In contrast, for relatively shallow networks, most notably one-hidden-layer ReLU models, training admits convex reformulations with global guarantees, motivating learning paradigms that improve stability while scaling to depth. MGDL builds upon this insight by training deep networks grade by grade: previously learned grades are frozen, and each new residual block is trained solely to reduce the remaining approximation error, yielding an interpretable and stable hierarchical refinement process. We develop an operator-theoretic foundation for MGDL and prove that, for any continuous target function, there exists a fixed-width multigrade ReLU scheme whose residuals decrease strictly across grades and converge uniformly to zero. To the best of our knowledge, this work provides the first rigorous theoretical guarantee that grade-wise training yields provable vanishing approximation error in deep networks. Numerical experiments further illustrate the theoretical results.

**Key words.** Multigrade Deep Learning, Structured Error Refinement, Balanced Contraction Operator, Deep Network Approximation

## 1 Introduction

Deep neural networks (DNNs) have achieved remarkable empirical success in areas such as computer vision, natural language processing, and scientific computing, owing to their strong expressive power for modeling complex input-output relationships. From an approximation-theoretic perspective, this expressive capacity is now relatively well understood: sufficiently deep and wide networks can approximate broad classes of functions with high accuracy [32, 38, 48]. Despite these advances, the effective training of deep neural networks with many layers is still not fully understood. Standard end-to-end training leads to highly non-convex and often ill-conditioned optimization landscapes, making performance sensitive to initialization, learning rates, and architectural choices. These challenges are further exacerbated by vanishing or exploding gradients, spectral bias toward low-frequency features [27, 47], and short-term oscillations near the edge of stability [1, 6]. In contrast, the optimization landscape of shallow architectures is fundamentally different; in particular, training one-hidden-layer ReLU networks can be reformulated as convex optimization problems, yielding global optimality and strong theoretical guarantees for both training and generalization [11, 26].

---

\* Corresponding author

This contrast reveals a fundamental dilemma: deep networks offer strong approximation power but are difficult to optimize, whereas shallow networks are easier to train but have limited expressive capacity. Motivated by this trade-off, multi-grade deep learning (MGDL) was introduced in [43]. The MGDL framework incrementally constructs network architectures via grade-wise training, aiming to combine the approximation advantages of deep networks with improved stability, accuracy, and interpretability. Specifically, MGDL decomposes end-to-end optimization into a sequence of smaller subproblems, each training a shallow network to approximate the residuals from previous grades. Networks learned at earlier grades are kept fixed and serve as adaptive basis functions or feature maps. This iterative refinement reduces optimization complexity while progressively improving approximation quality. While MGDL has demonstrated promising empirical performance and has been shown to achieve grade-wise training error reduction, a fundamental theoretical question remains open: whether such grade-wise training guarantees that the approximation error converges to zero in the limit. Addressing this gap is essential for establishing a rigorous theoretical foundation for the MGDL framework. The goal of this paper is to provide the first rigorous proof that, under suitable conditions, grade-wise training yields vanishing approximation error as grade number tends to infinity.

## 1.1 Multigrade deep learning

The central idea of MGDL is *grade-by-grade learning*: the network is constructed and trained one grade at a time, with only the newly added block optimized at each grade. All previously trained blocks are frozen and serve as adaptive basis components. Rather than learning the target function in a single global optimization, MGDL decomposes the task into a sequence of residual learning subproblems with progressively finer resolution. This recursive, coarse-to-fine structure promotes improved approximation and often results in more stable training dynamics.

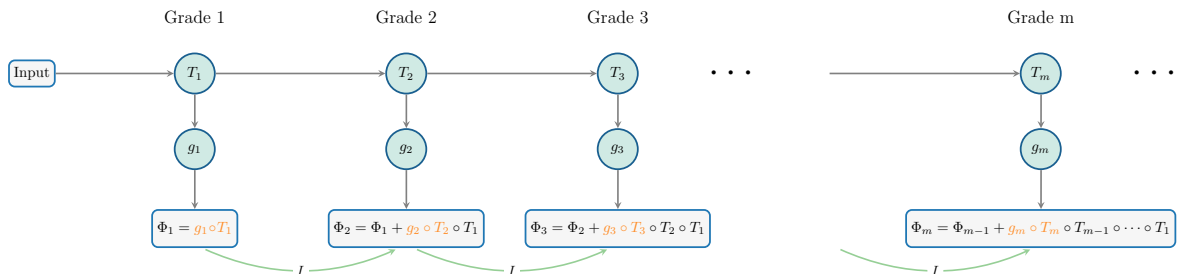


Figure 1: Overview of the MGDL framework and its grade-wise training procedure. Training proceeds grade by grade: at each grade, only the newly added block and the output map are optimized, while all previously learned blocks are frozen and serve as adaptive basis components. The network  $\Phi_m$  approximates the target function via a recursive residual refinement process.

As illustrated in Figure 1, each grade introduces a new learnable block while keeping all previously trained components fixed. At grade  $m$ , the module  $T_m$  serves as a feature transformation block, typically implemented as a shallow unit of the form  $\sigma \circ \mathcal{A}_m$ , where  $\mathcal{A}_m$  is an affine map and  $\sigma$  is a fixed activation. The accompanying map  $g_m$  is a simple output operator, often affine, that converts the transformed features into a correction term for the current residual.

Concretely, at grade  $m$  we *freeze* the previously learned blocks  $T_1, \dots, T_{m-1}$  and optimize only the new pair  $(T_m, g_m)$ . The objective is to train the composition

$$g_m \circ T_m \circ T_{m-1} \circ \dots \circ T_1$$

to best approximates the residual

$$R_{m-1} = f - \Phi_{m-1},$$

where  $\Phi_{m-1}$  denotes the approximation obtained from the first  $m-1$  grades. Once trained, the approximation is updated by

$$\Phi_m = \Phi_{m-1} + g_m \circ T_m \circ \cdots \circ T_1.$$

Thus, each grade solves a well-defined subproblem:  $T_m$  extracts new features based on all preceding transformations, and  $g_m$  fits the current residual using these features. A detailed algorithmic formulation of this grade-wise optimization procedure is provided in Section 2.

In particular, when each block  $T_i$  is chosen as a single-hidden-layer transformation of the form  $T_i = \sigma \circ \mathcal{A}_i$ , and each output map  $g_i$  is affine, denoted by  $\mathcal{A}_i^{\text{out}}$ , the grade-wise update takes the simplified form

$$\Phi_m = \Phi_{m-1} + \mathcal{A}_m^{\text{out}} \circ \sigma \circ \mathcal{A}_m \circ \cdots \circ \sigma \circ \mathcal{A}_1.$$

Consequently, the network obtained after  $m$  grades admits the explicit representation

$$\Phi_m = \sum_{\ell=1}^m \mathcal{A}_\ell^{\text{out}} \circ \bigcirc_{i=1}^{\ell} (\sigma \circ \mathcal{A}_i).$$

Here,  $\bigcirc$  denotes ordered composition: for a collection of maps  $\{f_i\}_{i=1}^n$ , we define

$$\bigcirc_{i=1}^n f_i := f_1 \circ f_2 \circ \cdots \circ f_n.$$

Viewed more broadly, MGDL departs fundamentally from standard end-to-end training by organizing deep network construction as a sequence of grade-wise residual refinements. At each grade, the newly introduced block is composed with all previously learned transformations, which remain frozen during training. This design preserves the full compositional expressive power of deep networks while decomposing learning into a sequence of controlled and interpretable subproblems. In contrast to classical approaches based on linear combinations of fixed basis functions, MGDL introduces adaptive, data-driven basis functions at each grade. These components are realized through additional layer compositions built upon frozen earlier transformations. As a result, the representational capacity grows in a structured and hierarchical manner, enabling progressively richer feature extraction while maintaining training stability and interpretability.

From both optimization and approximation perspectives, MGDL implements a divide-and-conquer strategy. Each grade solves a shallow residual learning problem, thereby reducing nonconvex interactions across layers, improving conditioning, and inducing a natural coarse-to-fine refinement mechanism in which dominant structures are captured first and finer details are resolved progressively. This hierarchical structure also facilitates theoretical analysis and, in certain settings, allows multigrade training to be interpreted as a sequence of simpler optimization problems, including *convex* formulations for shallow ReLU networks [11, 26].

Empirically, MGDL has demonstrated faster convergence, improved numerical stability, and enhanced approximation accuracy across regression, imaging, integral equations, and PDE-based applications [10, 11, 19, 43, 45]. Despite these empirical successes, and several theoretical observations concerning monotone training-error decay and reduced sensitivity of optimization convergence to learning rates, existing studies of MGDL remain largely experimental from an approximation-theoretic perspective. In particular, there is currently no rigorous theoretical framework that characterizes structural conditions under which the residual converges uniformly to zero. Establishing such guarantees is essential for elevating MGDL from a practical training paradigm to a principled approximation framework.

## 1.2 Main theorem

The main objective of this paper is to establish a rigorous theoretical foundation for MGDL. We develop an operator-theoretic perspective on the grade-wise refinement process and prove that, for a concrete class of fixed-width multigrade ReLU architectures, one can construct an MGDL scheme whose residuals decrease strictly at every grade and converge uniformly to the target function.

Throughout the paper, we use  $\text{Aff}_{\leq n}$  to denote the collection of all affine maps whose input and output dimensions are at most  $n$ :

$$\text{Aff}_{\leq n} := \bigcup_{1 \leq k \leq n} \bigcup_{1 \leq m \leq n} \{ \mathbf{x} \mapsto \mathbf{W}\mathbf{x} + \mathbf{b} : \mathbf{W} \in \mathbb{R}^{m \times k}, \mathbf{b} \in \mathbb{R}^m \}.$$

As usual,  $\mathbb{N}$ ,  $\mathbb{Z}$ , and  $\mathbb{R}$  denote the sets of natural numbers (including 0), integers, and real numbers, respectively, and we write

$$\mathbb{N}^+ := \mathbb{N} \setminus \{0\} = \{1, 2, 3, \dots\}.$$

For a domain  $\Omega \subseteq \mathbb{R}^d$ ,  $C(\Omega)$  denotes the space of real-valued continuous functions on  $\Omega$ . The symbol  $\sigma : \mathbb{R} \rightarrow \mathbb{R}$  denotes a fixed activation function, with ReLU being the primary example considered in this work. To describe monotone convergence, we write  $a_n \searrow a$  to denote a decreasing sequence converging to  $a$ , and say the convergence is “strictly” if  $a_{n+1} < a_n$  for all  $n$ . Additional notation will be introduced as needed.

We now state our main approximation theorem for MGDL.

**Theorem 1.1.** *Given  $f \in C([0, 1]^d)$ , there exist affine maps  $\mathcal{A}_i, \mathcal{A}_i^{\text{out}} \in \text{Aff}_{\leq 5d}$  for all  $i \in \mathbb{N}^+$  such that the sequence of multigrade approximations*

$$\Phi_k := \sum_{\ell=1}^k \mathcal{A}_\ell^{\text{out}} \circ \bigcirc_{i=1}^{\ell} (\text{ReLU} \circ \mathcal{A}_i) \quad \text{for } k \geq 1$$

generates residuals  $R_k := f - \Phi_k$  with the following properties:

- (i) For every  $\mathbf{x} \in [0, 1]^d$ ,  $|R_k(\mathbf{x})| \searrow 0$  as  $k \rightarrow \infty$ , and hence  $\|R_k\|_{L^\infty([0,1]^d)} \searrow 0$ .
- (ii) For any preassigned  $p \in [1, \infty)$ ,  $\|R_k\|_{L^p([0,1]^d)} \searrow 0$  strictly as  $k \rightarrow \infty$ .

The proof of Theorem 1.1 is presented in Section 3. We emphasize that the proof is fully constructive. More precisely, after a finite number of grades, determined by the complexity of the target function and a prescribed accuracy parameter  $\varepsilon \in (0, 1)$ , the residual admits an  $L^\infty$  contraction by a factor of  $1 - \varepsilon$ .

**Corollary 1.2.** *Given  $f \in C([0, 1]^d)$  and  $\varepsilon \in (0, 1)$ , there exists a subsequence  $\{k_j\}_{j=1}^\infty$ , constructed explicitly from  $f$  and  $\varepsilon$ , such that the residuals  $R_k$  in Theorem 1.1 satisfy*

$$\|R_{k_{j+1}}\|_{L^\infty([0,1]^d)} \leq (1 - \varepsilon) \|R_{k_j}\|_{L^\infty([0,1]^d)} \quad \text{for } j = 1, 2, \dots$$

We stress that the subsequence  $\{k_j\}_{j=1}^\infty$  in Corollary 1.2 is obtained through an explicit construction depending on  $f$  and  $\varepsilon$ , rather than by a purely existential argument, as will be evident from the proof of Theorem 1.1. To the best of our knowledge, these results provide the first rigorous theoretical foundation for MGDL as a principled framework for structured, grade-wise error refinement. They demonstrate that deep networks can be constructed incrementally through a sequence of residual corrections whose approximation errors decrease monotonically across successive grades, with strict contraction in every  $L^p$  norm for  $1 \leq p < \infty$ . This establishes a precise mechanism by which depth enables progressive refinement of approximation

accuracy and offers a concrete connection between MGDL training and classical approximation theory.

We emphasize that our analysis is carried out in the setting where the output map  $g$  is affine and each grade block  $T_i$  is given by the composition of an affine transformation with a fixed activation function. This formulation already covers a broad and practically relevant class of neural network architectures. The underlying ideas, however, are not intrinsically tied to this specific configuration. To illustrate this point, consider a simple extension in which each grade block  $T_i$  is implemented as a two-hidden-layer module of the form  $T_i = \text{ReLU} \circ \mathcal{A}_{2i} \circ \text{ReLU} \circ \mathcal{A}_{2i-1}$ , rather than a single-hidden-layer block  $\text{ReLU} \circ \mathcal{A}_i$ . The same analytical strategy can be applied in this setting. In particular, if approximation efficiency is not the primary concern, one may effectively render the intermediate component  $\text{ReLU} \circ \mathcal{A}_{2i}$  inactive by choosing it to implement an identity map. This is possible, for instance, using the identity  $\text{ReLU}(x) - \text{ReLU}(-x) = x$ , which allows the additional layer to be absorbed without altering the overall mapping. More generally, extensions to richer choices of output maps and block structures are expected to follow similar lines of reasoning, although they would require handling a substantially larger class of architectures. A systematic treatment of such generalizations is beyond the scope of the present work and is therefore left for future investigation. To further elucidate the implications of Theorem 1.1, we next interpret the MGDL framework from the perspective of dictionary-based approximation.

### 1.3 Understanding MGDL from dictionary-based approximation

From the viewpoint of dictionary-based approximation, the MGDL refinement process admits a natural interpretation in terms of basis expansions and sparse approximation. These paradigms provide a conceptual framework for understanding the mechanism of progressive error reduction that underlies grade-wise training.

#### Basis expansions

Classical basis expansions provide a conceptually straightforward framework for function approximation, with Fourier-type expansions serving as a canonical example. Given a prescribed and fixed collection of basis functions, approximation is achieved by selecting basis elements, often in a predetermined or hierarchical order, and forming linear combinations to approximate the target function. Typically, the approximation accuracy improves, as additional basis elements are included. However, because the basis is fixed a priori and does not adapt to the specific structure of the target function, such approaches can be inefficient when the target exhibits complex, anisotropic, or highly localized features.

#### Sparse approximation

Sparse approximation adopts a more flexible, but technically more involved, approach. Instead of relying on a basis, it employs a *dictionary*, typically a redundant system, such as multiresolution-analysis-based wavelet tight frames in  $L^2(\mathbb{R}^d)$  [29]. Given a dictionary  $\mathcal{D} = \{\mathbf{e}_i\}_{i \in \mathcal{I}}$ , the goal is to approximate a target function using only a small number of dictionary elements. A standard greedy strategy proceeds by iteratively reducing the residual. Starting from  $R_0 = f$ , one selects at each iteration an atom–coefficient pair by solving

$$(\alpha_{k+1}, \mathbf{e}_{i_{k+1}}) \in \arg \min_{\alpha \in \mathbb{R}, \mathbf{e} \in \mathcal{D}} \|R_k - \alpha \mathbf{e}\|,$$

with respect to a chosen norm, and updates the residual via  $R_{k+1} = R_k - \alpha_{k+1} \mathbf{e}_{i_{k+1}}$ . Each iteration extracts the dictionary element that best explains the current residual, leading to a monotone refinement of the approximation. While sparse approximation is highly effective, its

performance typically depends on the availability of a sufficiently rich dictionary, often requiring a large number of atoms to achieve high accuracy.

### Neural networks with end-to-end training

From the sparse approximation viewpoint, standard end-to-end neural network training can be interpreted as a single-step approximation problem over a highly expressive dictionary. Specifically, one may regard the neural network dictionary as

$$\mathcal{D}_{\text{NN}} = \{T_m \circ \cdots \circ T_1 : T_1, \dots, T_m \text{ are network blocks}\},$$

for a chosen sufficiently large  $m \in \mathbb{N}^+$ . This dictionary consists of a large family of parameterized compositional maps. End-to-end training then amounts to selecting a single element from this dictionary together with an output map  $g \in \mathcal{G}$  by solving

$$(g^*, \mathbf{e}^*) \in \arg \min_{g \in \mathcal{G}, \mathbf{e} \in \mathcal{D}_{\text{NN}}} \|f - g \circ \mathbf{e}\|.$$

The resulting approximation takes the form

$$f \approx g^* \circ \mathbf{e}^* = g^* \circ T_m^* \circ \cdots \circ T_1^*.$$

Although the dictionary  $\mathcal{D}_{\text{NN}}$  is, in principle, highly expressive, this formulation highlights the intrinsic difficulty of end-to-end learning. Selecting a single, highly structured element from an extremely large and nonconvex dictionary is inherently challenging, as approximation errors must be coordinated across all layers simultaneously. This coupling often leads to severe optimization difficulties and unstable training dynamics, despite the strong representational capacity of the underlying dictionary.

### MGDL viewpoint

MGDL combines key advantages of sparse approximation and neural network-based representations. On the one hand, it retains a highly expressive dictionary generated by deep compositions. On the other hand, it replaces the single-shot selection of an entire network with a sequence of simple, structured greedy steps.

More precisely, MGDL constructs the compositional dictionary

$$\mathcal{D}_{\text{MGDL}} = \left\{ \bigcirc_{i=1}^k T_i : k \in \mathbb{N}^+, \quad T_1, T_2, \dots \text{ are network blocks} \right\}.$$

For notational convenience, we denote by  $\mathcal{D}_{\text{MGDL}}(k)$  the subset of  $\mathcal{D}_{\text{MGDL}}$  consisting of compositions of the form  $T_k \circ \cdots \circ T_1$ .

Starting from  $R_0 = f$ , MGDL proceeds iteratively by selecting, at each grade, an atom together with an output map  $g \in \mathcal{G}$  through the optimization problem

$$(g_{k+1}, \mathbf{e}_{k+1}) \in \arg \min_{g \in \mathcal{G}, \mathbf{e} \in \mathcal{D}_{\text{MGDL}}(k)} \|R_k - g \circ \mathbf{e}\|.$$

The residual is then updated according to

$$R_{k+1} := R_k - g_{k+1} \circ \mathbf{e}_{k+1}.$$

Crucially, at each iteration only the newly introduced block  $T_k$  and the output map  $g_k$  are optimized, while all previously learned blocks remain fixed. As a result, each step involves a relatively simple optimization problem, yet the overall approximation benefits from an adaptively growing and highly expressive compositional dictionary. This structure enables monotone

residual refinement while substantially easing the optimization burden compared with standard end-to-end training.

Finally, it is important to note that after  $k - 1$  iterations, the composition  $T_{k-1} \circ \dots \circ T_1$  already provides a near-optimal representation within the current compositional class, in the sense that the corresponding residual  $R_{k-1}$  cannot be significantly reduced by further optimizing within the same functional space. Simply selecting another atom from this fixed space would therefore yield only marginal improvement. Introducing a new block  $T_k$  effectively enlarges representation space, expanding the dictionary and creating new directions along which the residual can be reduced. This mechanism explains why each new grade can yield a substantial error decrease, despite the greedy nature of the construction.

## 1.4 Related work

The present work is closely related to several active research directions in neural network approximation theory and learning theory. Below, we briefly review representative developments on expressive power, frequency-based perspectives on learnability, and hierarchical or multigrade training strategies, and clarify how our results differ from and complement existing approaches.

### Expressive power of neural networks

The expressive capacity of neural networks has been a central topic in approximation theory and learning theory. Classical universal approximation results [7, 16, 17] establish that even shallow neural networks can approximate arbitrary continuous functions on compact domains. While foundational, these results are qualitative in nature and do not quantify how network size, depth, or architectural constraints affect approximation efficiency. Subsequent research has significantly refined this theory by deriving sharp approximation rates for specific function classes and by elucidating the roles of depth, width, and compositional structure in determining representational efficiency [2, 5, 12, 13, 21, 22, 24, 32, 35, 38, 39, 48, 49, 50, 52, 56].

More recently, deep learning in reproducing kernel Banach spaces (RKBS) was introduced in [42], where deep neural networks are interpreted as asymmetric kernels with respect to the input and parameter variables. This viewpoint recasts deep learning as a form of kernel-based learning in RKBS, extending the classical reproducing kernel Hilbert space framework, and yields representer theorems for deep architectures. In parallel, a growing body of work has explored novel architectures and activation functions aimed at enhancing approximation power or reducing model complexity [33, 34, 36, 37, 41, 51, 53]. Despite this substantial progress, most of the existing literature focuses primarily on representational capacity. Fundamental questions concerning *learnability*, optimization dynamics, and the gap between expressivity and effective training remain largely unresolved [30, 31, 40, 55].

### Frequency-based perspectives on learnability

Motivated by the gap between expressivity and practical trainability, a complementary line of research examines neural network learning from a frequency-based perspective [3, 23, 28, 46, 54, 55]. A central concept in this direction is the *frequency principle* [23, 46], which posits that neural networks tend to fit low-frequency components of a target function earlier than high-frequency ones during training. This phenomenon has been empirically observed across a wide range of architectures and learning tasks, and has inspired theoretical studies linking optimization dynamics, spectral bias, and generalization. Nevertheless, existing results are largely qualitative or problem-dependent, and a rigorous, architecture-level theory that systematically characterizes frequency-dependent learnability is still lacking.

## Hierarchical, residual, and multigrade training strategies

A closely related line of work studies architectural and algorithmic mechanisms that promote stable optimization and progressive error refinement. Residual learning [14], layerwise or greedy training schemes [4, 15], and hierarchical forecasting or refinement architectures [8, 9, 25] have all demonstrated empirical success in improving convergence behavior and mitigating optimization difficulties. Within this context, the MGDL framework was introduced empirically in [43] to enhance training stability, accelerate convergence, and alleviate optimization pathologies such as vanishing gradients. A specialized variant of MGDL was later proposed in [44] in the form of the successive affine learning model, where each affine transformation is first learned by solving a quadratic or convex optimization problem, and the activation function is applied only after the weight matrix and bias vector of the current layer are determined. While related coarse-to-fine and multilevel strategies have shown strong performance across regression, imaging, integral equation and PDE-solving tasks [10, 11, 18, 19, 43], existing analyses remain largely empirical. Consequently, they lack rigorous guarantees that grade-wise residuals will converge uniformly to zero within concrete neural network architectures.

Despite promising empirical evidence for hierarchical and residual methods, none of the aforementioned approaches, including the original MGDL study [43], establishes a rigorous approximation theory that guarantees *uniform convergence* in an explicit neural network construction. This work fills that gap. We develop an operator-theoretic formulation of MGDL and identifying the structural conditions under which a fixed-width, multigrade ReLU architecture admits a grade-wise optimization scheme. We prove that this scheme produces strictly decreasing residuals that converge uniformly to zero. These results provide the first theoretical foundation for MGDL as a principled framework for structured error refinement, bridging the gap between classical expressivity theory and modern hierarchical learning.

The remainder of this paper is organized as follows. Section 2 describes the MGDL framework, including the grade-wise optimization algorithm and numerical experiments that illustrate the theoretical results, as well as its practical performance and advantages over standard end-to-end training. Section 3 presents the proof of the main approximation result, Theorem 1.1, which is established assuming the auxiliary one-step contraction result, Theorem 3.1. The proof of this auxiliary theorem is given in Section 4, where we develop the core technical construction underlying the one-step contraction through a detailed operator-theoretic analysis and its realization by fixed-width ReLU networks. Finally, Section 5 concludes the paper and discusses possible directions for future work.

## 2 MGDL algorithm and experiments

In this section, we first describe the concrete realization of the MGDL framework, following [43], together with its grade-wise learning algorithm in Section 2.1. We then present numerical experiments illustrating its practical behavior in Section 2.2.

### 2.1 Grade-wise optimization

We begin by formulating the MGDL learning process at the function level. Let the target be a (vector-valued) function  $f$ , and let  $T_i$  denote a parameterized network block, for example  $T_i = \sigma \circ \mathcal{A}_i$  with an activation function  $\sigma$  and an affine map  $\mathcal{A}_i$ . Let  $g_i$  denote a parameterized output map, such as an affine transformation that ensures dimensional consistency with the target.

As illustrated in Figure 1, MGDL constructs the network grade by grade.

- **Grade 1.** Train  $\Phi_1 = g_1 \circ T_1$  to approximate  $f$ . The first residual is  $R_1 = f - \Phi_1$ .

- **Grade 2.** Freeze  $T_1$  and train a new block  $T_2$  together with an output map  $g_2$  so that  $g_2 \circ T_2 \circ T_1$  approximates the residual  $R_1$ . The updated approximation is

$$\Phi_2 = \Phi_1 + g_2 \circ T_2 \circ T_1,$$

and the new residual is given by  $R_2 = f - \Phi_2$ .

- **Higher grades.** Proceeding inductively, at grade  $m \geq 3$  we fix  $T_1, \dots, T_{m-1}$ , introduce a new block  $T_m$  and an output map  $g_m$ , and train  $g_m \circ T_m \circ T_{m-1} \circ \dots \circ T_1$  to approximate the residual  $R_{m-1} = f - \Phi_{m-1}$ . The grade  $m$  approximant becomes

$$\Phi_m = \Phi_{m-1} + g_m \circ T_m \circ T_{m-1} \circ \dots \circ T_1,$$

and the residual is updated to  $R_m = f - \Phi_m$ .

After  $m$  grades, the overall MGDL approximant can be written as

$$\Phi_m = \sum_{k=1}^m g_k \circ T_k \circ T_{k-1} \circ \dots \circ T_1,$$

where  $T_1$  acts on the original input. As  $m$  increases, the approximation is refined recursively, and the central question is whether the residuals  $R_m$  can be guaranteed to decrease monotonically and converge to zero under suitable architectural choices. Theorem 1.1 provides an affirmative answer for a class of fixed-width multigrade ReLU networks.

The same construction can be expressed directly in terms of the training data. Suppose we are given samples  $\{(\mathbf{x}_i, f(\mathbf{x}_i))\}_{i=1}^N$ . For convenience, set

$$\mathbf{x}_i^{(1)} := \mathbf{x}_i, \quad y_i^{(1)} := f(\mathbf{x}_i^{(1)}).$$

The first grade learns a shallow network  $\Phi_1 = g_1 \circ T_1$  by solving

$$\min_{g_1, T_1} \frac{1}{N} \sum_{i=1}^N \ell(g_1 \circ T_1(\mathbf{x}_i^{(1)}), y_i^{(1)}),$$

which yields the first approximation  $\Phi_1 = g_1 \circ T_1$ . We then define the transformed inputs and residual outputs

$$\mathbf{x}_i^{(2)} := T_1(\mathbf{x}_i^{(1)}), \quad y_i^{(2)} := y_i^{(1)} - g_1 \circ T_1(\mathbf{x}_i^{(1)}).$$

At grade 2, the block  $T_1$  is fixed, and we solve

$$\min_{g_2, T_2} \frac{1}{N} \sum_{i=1}^N \ell(g_2 \circ T_2(\mathbf{x}_i^{(2)}), y_i^{(2)}).$$

In general, at grade  $m$ , we define

$$\mathbf{x}_i^{(m)} := T_{m-1} \circ \dots \circ T_1(\mathbf{x}_i), \quad y_i^{(m)} := y_i^{(m-1)} - g_{m-1} \circ T_{m-1}(\mathbf{x}_i^{(m-1)}),$$

freezes  $T_1, \dots, T_{m-1}$ , and solves the grade-wise problem

$$\min_{g_m, T_m} \frac{1}{N} \sum_{i=1}^N \ell(g_m \circ T_m(\mathbf{x}_i^{(m)}), y_i^{(m)}).$$

Thus, at grade  $m$  the learning task focuses on capturing the current residual through  $g_m \circ T_m$  using the data  $\{(\mathbf{x}_i^{(m)}, y_i^{(m)})\}_{i=1}^N$ , rather than reoptimizing all layers simultaneously as in end-to-end training. This grade-wise formulation makes the recursive refinement structure explicit and aligns directly with the operator-theoretic framework underlying Theorem 1.1.

## 2.2 Numerical experiments

The purpose of this subsection is to illustrate the main theoretical results on MGDL presented in Section 1, in particular the progressive decay of approximation residuals to zero across successive grades. Through numerical experiments in one and two spatial dimensions, we examine whether the residual error decreases consistently as the grade index increases, and whether the activation of each new grade yields a substantial and stable improvement in approximation accuracy. These empirical observations directly reflect the grade-wise residual refinement principle developed in the theoretical analysis. As a supplementary reference, comparisons with standard end-to-end training are reported at the end of this section.

### Target functions

We consider target functions with pronounced high-frequency components and nonlinear couplings. In one dimension, the target function is

$$f_1(x) = \sin(32\pi x) - 0.5 \cos(16\pi x^2).$$

In two dimensions, we use the coupled oscillatory function

$$f_2(x_1, x_2) = \sum_{i=1}^2 \sum_{j=1}^2 a_{i,j} \sin(b_i x_i + c_{i,j} x_i x_j) |\cos(d_j x_j + e_{i,j} x_i^2)|,$$

where

$$(a_{i,j}) = \begin{bmatrix} 0.3 & 0.2 \\ 0.2 & 0.3 \end{bmatrix}, \quad (b_i) = \begin{bmatrix} 12\pi \\ 8\pi \end{bmatrix}, \quad (c_{i,j}) = \begin{bmatrix} 4\pi & 12\pi \\ 6\pi & 10\pi \end{bmatrix}, \quad (d_j) = \begin{bmatrix} 14\pi & 12\pi \\ 8\pi & 10\pi \end{bmatrix}.$$

Figure 2 and Figure 3 visualize the target functions  $f_1$  and  $f_2$ .

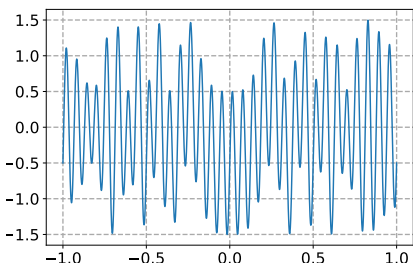


Figure 2: 1D target function  $f_1$ .

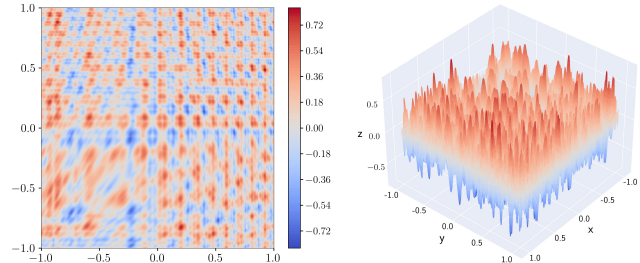


Figure 3: 2D target function  $f_2$ .

### Training protocol, data, and MGDL architectures

All experiments are implemented in PyTorch and optimized using the Adam optimizer [20]. Training is conducted in single precision by minimizing the mean-squared error (MSE). Network parameters are initialized using PyTorch’s default uniform initialization  $\mathcal{U}(-\sqrt{k}, \sqrt{k})$  with  $k$  being set as the reciprocal of the input feature dimension, applied to both weights and biases.

For the one-dimensional experiment, 10,000 training samples are drawn independently from the uniform distribution on  $[-1, 1]$  and trained with mini-batch size 400. Test errors are evaluated using 3,000 fresh samples drawn from the same distribution. For the two-dimensional experiment, training is performed on a uniform Cartesian grid of size  $500 \times 500$  over  $[-1, 1]^2$  with mini-batch size 1,000. Test errors are computed using 90,000 points sampled independently and uniformly from  $[-1, 1]^2$ .

We now describe the MGDL architectures and their grade-wise training strategy, with emphasis on how residual errors evolve across successive grades.

- The one-dimensional MGDL model takes the form

$$\sum_{\ell=1}^4 \mathcal{A}_\ell^{\text{out}} \circ \bigcirc_{i=1}^{\ell} (\text{ReLU} \circ \mathcal{A}_{2i} \circ \text{ReLU} \circ \mathcal{A}_{2i-1}),$$

with split layers (2, 4, 6, 8). At grade  $\ell$ , only the newly introduced affine maps  $\mathcal{A}_{2\ell-1}$ ,  $\mathcal{A}_{2\ell}$ , and  $\mathcal{A}_\ell^{\text{out}}$  are optimized, while all previously trained components are kept frozen. A total of 12,000 training epochs are distributed across grades as (750, 1500, 3000, 6750). At each grade, the learning rate follows the schedule  $\eta_k = \eta_0 0.9^{\lfloor k/s \rfloor}$  with  $\eta_0 = 0.001$  and  $s = 120$ .

- The two-dimensional MGDL model follows the same multigrade paradigm and is given by

$$\sum_{\ell=1}^3 \mathcal{A}_\ell^{\text{out}} \circ \bigcirc_{i=1}^{\ell} (\text{ReLU} \circ \mathcal{A}_{3i} \circ \text{ReLU} \circ \mathcal{A}_{3i-1} \circ \text{ReLU} \circ \mathcal{A}_{3i-2}),$$

with split layers (3, 6, 9). Training is performed for a total of 1,200 epochs, allocated across grades as (150, 300, 750). At each grade, the learning rate at epoch  $k$  is given by  $\eta_k = \eta_0 0.9^{\lfloor k/s \rfloor}$ , where  $\eta_0 = 0.001$  and  $s = 12$ .

### Grade-wise residual decay

Figure 4 displays the evolution of training and test errors, with shaded regions indicating individual grades. For completeness, we also report test errors measured in the  $\ell^\infty$  norm (MAX). In both the experiments of one and two dimensions, the error curves exhibit a clear grade-wise structure. At the onset of each new grade, the residual error undergoes a pronounced drop, followed by a stable decay as training proceeds within that grade. Across successive grades, the residual consistently decreases and approaches zero.

Importantly, the most significant reductions occur immediately after activating a new grade, indicating that each grade contributes a nontrivial refinement of the approximation. This behavior is highly consistent across dimensions and target functions, and provides strong empirical support for viewing MGDL as a structured residual correction process, in close agreement with the theoretical results.

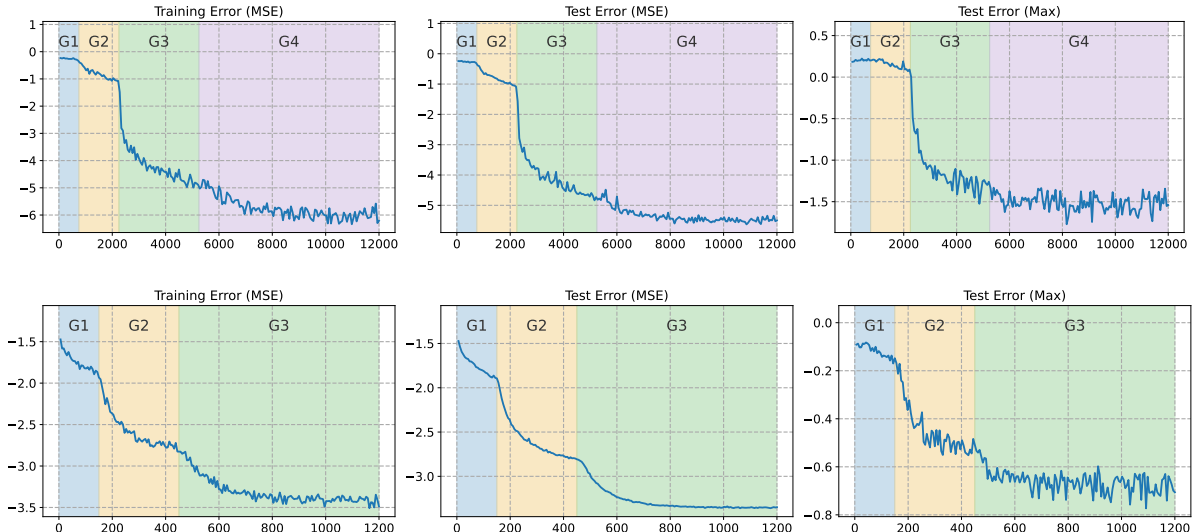


Figure 4: Error curves for  $f_1$  (top row) and  $f_2$  (bottom row). Shaded regions indicate individual grades (G1–G4 for  $f_1$  and G1–G3 for  $f_2$ ). The horizontal axis denotes training epochs, and the vertical axis shows the base-10 logarithm of the error.

## Supplementary comparison with end-to-end training

For completeness, we also report results obtained from standard fully connected neural networks (FCNNs) trained end to end. The FCNN baselines are designed to ensure a fair and controlled comparison: they use the same activation functions, network width, and overall depth as the MGDL trunk, and are trained for the same total number of epochs under identical optimization settings, including the optimizer, learning rate schedule, batch size, and data sampling strategy. More specifically, in the one-dimensional experiment, all FCNN parameters are optimized simultaneously for 12,000 epochs. The learning rate at epoch  $k$  follows the schedule  $\eta_k = \eta_0 0.9^{\lfloor k/s \rfloor}$  with  $\eta_0 = 0.001$  and step size  $s = 200$ . In the two-dimensional experiment, all parameters are optimized simultaneously for 1,200 epochs, using the same learning-rate decay rule with  $\eta_0 = 0.001$  and step size  $s = 20$ .

Table 1: Final error comparison between the end-to-end FCNN baseline and MGDL model.

	training error (MSE)		test error (MSE)		test error (MAX)	
	FCNN	MGDL	FCNN	MGDL	FCNN	MGDL
1D ( $f_1$ )	$5.54 \times 10^{-5}$	$1.25 \times 10^{-6}$	$6.14 \times 10^{-5}$	$3.56 \times 10^{-6}$	$1.03 \times 10^{-1}$	$3.41 \times 10^{-2}$
2D ( $f_2$ )	$8.78 \times 10^{-4}$	$3.89 \times 10^{-4}$	$8.14 \times 10^{-4}$	$4.47 \times 10^{-4}$	$4.06 \times 10^{-1}$	$2.03 \times 10^{-1}$

Final training and test errors are summarized in Table 1, while the comparison of the error curves is shown in Figure 5. Although both models are trained under matched experimental conditions, MGDL consistently achieves substantially lower training and test errors than the end-to-end FCNN baseline. These results demonstrate that the structured grade-wise residual refinement strategy of MGDL is markedly more effective at reducing approximation errors than standard end-to-end training, especially for functions with strong high-frequency content and nonlinear coupling.

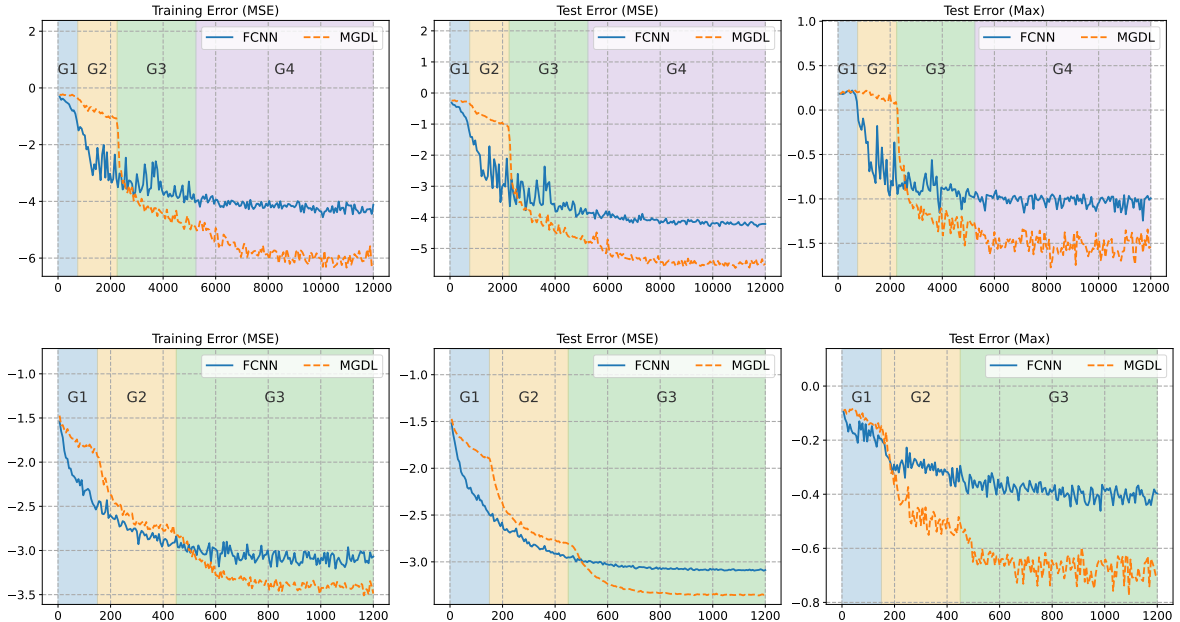


Figure 5: Comparison of FCNN and MGDL via error curves for  $f_1$  (top row) and  $f_2$  (bottom row). Shaded bands indicate individual grades (G1–G4 for  $f_1$  and G–G3 for  $f_2$ ). The horizontal axis represents training epochs, and the vertical axis displays the base-10 logarithm of the error.

### 3 Proof of Theorem 1.1

The purpose of this section is to establish the main approximation result, Theorem 1.1, stated in Section 1.2. We begin in Section 3.1 with an overview of the proof strategy, highlighting the key ideas and the operator-theoretic structure underlying the argument. The detailed construction and complete proof of Theorem 1.1 are then presented in Section 3.2.

#### 3.1 Proof strategy

The proof of Theorem 1.1 proceeds in two-steps. First, we construct a nonlinear operator  $S$  on  $C([0, 1]^d)$ , realizable by a ReLU network, such that for every target function  $g$ , we have a uniform contraction

$$\|g - Sg\|_{L^\infty([0,1]^d)} \leq (1 - \varepsilon) \|g\|_{L^\infty([0,1]^d)},$$

where  $\varepsilon \in (0, 1)$  depends only on the dimension  $d$ . Second, we apply this contraction iteratively to the residuals of the MGDL residuals, which yields geometric decay and thereby establishes Theorem 1.1. The first step constitutes the main technical contribution and is formalized in the following theorem.

**Theorem 3.1.** *Let  $f \in C([0, 1]^d)$  be given. There exist  $n \in \mathbb{N}^+$  and affine maps  $\mathcal{A}_i, \mathcal{A}_i^{\text{out}} \in \text{Aff}_{\leq 5d}$  for  $i = 1, 2, \dots, n$  such that, defining  $f_1 := f$  and*

$$f_{k+1} := f_k - \mathcal{A}_k^{\text{out}} \circ \bigcirc_{i=1}^k (\text{ReLU} \circ \mathcal{A}_i) \quad \text{for } k = 1, 2, \dots, n,$$

the following properties hold:

(i) Uniform accuracy:

$$\|f_{n+1}\|_{L^\infty([0,1]^d)} \leq (1 - \varepsilon) \|f\|_{L^\infty([0,1]^d)}$$

for any prescribed  $\varepsilon \in (0, \frac{1}{1+2^d})$ .

(ii) Pointwise domination:

$$|f_{k+1}(\mathbf{x})| \leq |f_k(\mathbf{x})| \quad \text{for all } \mathbf{x} \in [0, 1]^d \quad \text{and } k = 1, 2, \dots, n.$$

(iii) Strict  $L^p$  monotonicity: for any  $p \in [1, \infty)$ :

$$\|f_{k+1}\|_{L^p([0,1]^d)} < \|f_k\|_{L^p([0,1]^d)} \quad \text{for } k = 1, 2, \dots, n.$$

The proof of Theorem 3.1 is presented in Section 4. Within the MGDL framework, the operator  $S$  is realized by the multigrade ReLU construction of Theorem 3.1. Iterative application of this contraction to the MGDL residuals yields the grade-wise error decay claimed in Theorem 1.1.

#### 3.2 Main argument

With Theorem 3.1 in place, Theorem 1.1 follows by iteratively applying the one-step contraction to the successive residuals. This argument directly mirrors the MGDL refinement process, with the operators constructed in Theorem 3.1 serving as the grade-wise subnetworks.

*Proof of Theorem 1.1.* Apply Theorem 3.1 to  $f_1 := f \in C([0, 1]^d)$ . There exist  $n_1 \in \mathbb{N}^+$  and affine maps  $\mathcal{A}_i, \mathcal{A}_i^{\text{out}} \in \text{Aff}_{\leq 5d}$  for  $i = 1, 2, \dots, n_1$  such that, with

$$f_{k+1} := f_k - \mathcal{A}_k^{\text{out}} \circ \bigcirc_{i=1}^k (\text{ReLU} \circ \mathcal{A}_i) \quad \text{for } k = 1, 2, \dots, n_1,$$

the following properties are satisfied:

(i) Uniform accuracy:

$$\|f_{n_1+1}\|_{L^\infty([0,1]^d)} \leq (1 - \varepsilon) \|f_1\|_{L^\infty([0,1]^d)}.$$

(ii) Pointwise domination:

$$|f_{k+1}(\mathbf{x})| \leq |f_k(\mathbf{x})| \quad \text{for all } \mathbf{x} \in [0, 1]^d \text{ and } k = 1, 2, \dots, n_1.$$

(iii) Strict  $L^p$  monotonicity for every  $p \in [1, \infty)$ :

$$\|f_{k+1}\|_{L^p([0,1]^d)} < \|f_k\|_{L^p([0,1]^d)} \quad \text{for } k = 1, 2, \dots, n_1.$$

Next, apply Theorem 3.1 again to  $f_{n_1+1} \in C([0, 1]^d)$ . There exist  $n_2 \in \mathbb{N}^+$  and affine maps  $\mathcal{A}_k, \mathcal{A}_k^{\text{out}} \in \text{Aff}_{\leq 5d}$  for  $k = n_1 + 1, \dots, n_1 + n_2$  such that, with

$$f_{k+1} := f_k - \mathcal{A}_k^{\text{out}} \circ \bigcirc_{i=1}^k (\text{ReLU} \circ \mathcal{A}_i) \quad \text{for } k = n_1 + 1, \dots, n_1 + n_2,$$

the following properties hold:

(i) Uniform accuracy:

$$\|f_{n_1+n_2+1}\|_{L^\infty([0,1]^d)} \leq (1 - \varepsilon) \|f_{n_1+1}\|_{L^\infty([0,1]^d)} \leq (1 - \varepsilon)^2 \|f_1\|_{L^\infty([0,1]^d)}.$$

(ii) Pointwise domination:

$$|f_{k+1}(\mathbf{x})| \leq |f_k(\mathbf{x})| \quad \text{for all } \mathbf{x} \in [0, 1]^d \text{ and } k = 1, 2, \dots, n_1 + n_2.$$

(iii) Strict  $L^p$  monotonicity:

$$\|f_{k+1}\|_{L^p([0,1]^d)} < \|f_k\|_{L^p([0,1]^d)} \quad \text{for } k = 1, 2, \dots, n_1 + n_2.$$

Proceeding recursively, the same argument can be applied to  $f_{n_1+n_2+1}, f_{n_1+n_2+n_3+1}$ , and so on. By this iterative construction, affine maps  $\mathcal{A}_i, \mathcal{A}_i^{\text{out}} \in \text{Aff}_{\leq 5d}$ , for  $i = 1, 2, \dots$ , can be obtained such that, with

$$f_{k+1} := f_k - \mathcal{A}_k^{\text{out}} \circ \bigcirc_{i=1}^k (\text{ReLU} \circ \mathcal{A}_i) \quad \text{for } k = 1, 2, \dots,$$

the following properties are satisfied:

(i) Uniform accuracy:

$$\|f_k\|_{L^\infty([0,1]^d)} \rightarrow 0 \quad \text{as } k \rightarrow \infty.$$

(ii) Pointwise domination:

$$|f_{k+1}(\mathbf{x})| \leq |f_k(\mathbf{x})| \quad \text{for all } \mathbf{x} \in [0, 1]^d \text{ and } k = 1, 2, \dots.$$

(iii) Strict  $L^p$  monotonicity for every  $p \in [1, \infty)$ :

$$\|f_{k+1}\|_{L^p([0,1]^d)} < \|f_k\|_{L^p([0,1]^d)} \quad \text{for } k = 1, 2, \dots.$$

Finally, define the residual sequence

$$R_k := f - \Phi_k \quad \text{and} \quad \Phi_k := \sum_{\ell=1}^k \mathcal{A}_\ell^{\text{out}} \circ \bigcirc_{i=1}^{\ell} (\text{ReLU} \circ \mathcal{A}_i) \quad \text{for all } k \in \mathbb{N}^+.$$

By construction and the recursive definition of  $\{f_k\}$ , one readily verifies that

$$R_k = f_{k+1} \quad \text{for all } k \in \mathbb{N}^+.$$

Consequently, all properties established for  $\{f_k\}_{k=1}^\infty$  immediately carry over to the residual sequence  $\{R_k\}_{k=1}^\infty$ . In particular, we have

$$\|R_k\|_{L^\infty([0,1]^d)} \rightarrow 0 \quad \text{as } k \rightarrow \infty,$$

together with the pointwise monotonicity

$$|R_{k+1}(\mathbf{x})| \leq |R_k(\mathbf{x})| \quad \text{for all } \mathbf{x} \in [0, 1]^d \text{ and } k \in \mathbb{N}^+,$$

and the strict monotonic decrease in every  $L^p$  norm for  $p \in [1, \infty)$ ,

$$\|R_{k+1}\|_{L^p([0,1]^d)} < \|R_k\|_{L^p([0,1]^d)} \quad \text{for all } k \in \mathbb{N}^+.$$

Since  $|R_k(\mathbf{x})| \leq \|R_k\|_{L^\infty([0,1]^d)}$  for all  $\mathbf{x} \in [0, 1]^d$ , the uniform convergence implies

$$|R_k(\mathbf{x})| \searrow 0 \quad \text{as } k \rightarrow \infty \text{ for every } \mathbf{x} \in [0, 1]^d.$$

We remark that, in Corollary 1.2, the subsequence  $\{k_j\}_{j=1}^\infty$  can be constructed in the form

$$k_j = \sum_{i=1}^j n_i,$$

where each  $n_i$  depends on the target function  $f$  and the prescribed  $\varepsilon$ . The explicit construction will be clarified in the proof of Theorem 3.1.

Moreover, the inequality

$$\|R_k\|_{L^p([0,1]^d)} \leq \|R_k\|_{L^\infty([0,1]^d)}$$

combined with the strict  $L^p$  monotonicity yields

$$\|R_k\|_{L^p([0,1]^d)} \searrow 0 \text{ strictly} \quad \text{as } k \rightarrow \infty.$$

This completes the proof. □

## 4 Proof of Theorem 3.1

In this section, we present a complete proof of Theorem 3.1. We begin by outlining the proof strategy in Section 4.1. Next, Section 4.2 introduces the necessary preliminaries, including the relevant contraction notions, auxiliary lemmas, and structural conditions that will be used throughout the proof. Finally, these components are assembled in Section 4.3 to establish the desired one-step contraction, thereby completing the proof.

## 4.1 Proof strategy

We summarize here the proof strategy for Theorem 3.1 and outline the construction that leads to the desired one-step contraction. Given a target function  $g$  and a prescribed proportion parameter  $\varepsilon \in (0, 1)$ , the argument proceeds through the following three conceptual steps.

*Step 1: Localization of the near-maximum region.*

We first identify the subset on which  $|g|$  is close to its supremum, namely,

$$E_{g,\varepsilon} := \{ \mathbf{x} \in [0, 1]^d : |g(\mathbf{x})| \geq (1 - \varepsilon) \|g\|_{L^\infty([0,1]^d)} \}.$$

Figure 6 illustrates the region  $E_{g,\varepsilon}$ . This set is then covered by finitely many essentially disjoint hypercubes, ensuring that a strictly positive proportion of the residual mass is localized within geometrically simple, well-structured regions.

*Step 2: Construction of cutoff functions.*

For each hypercube  $Q$  in the above cover, we construct a continuous cutoff function that

- (i) attains the constant value  $\varepsilon \|g\|_{L^\infty([0,1]^d)}$  on  $Q$ ,
- (ii) decays continuously to zero on a slightly enlarged cube, and
- (iii) vanishes identically outside this enlargement.

Each such cutoff function can be implemented exactly by a shallow ReLU network. Figure 6 schematically illustrates this construction.

*Step 3: Assembly of the contraction operator.*

We define the operator  $Sg$  as the signed sum of all cutoff functions, with the amplitudes scaled so that  $Sg$  is sign-aligned with  $g$  and satisfies the pointwise bound

$$|Sg(\mathbf{x})| \leq |g(\mathbf{x})| \quad \text{for all } \mathbf{x}.$$

To guarantee this inequality, we carefully account for potential overlaps among the supports of the cutoff functions as illustrated in Figure 6 and choose the contraction parameter  $\varepsilon$  sufficiently small so that the aggregate contribution of all cutoffs remains dominated by  $|g|$ . Under our construction, the number of overlapping cutoff supports at any point is uniformly bounded by  $2^d$ , as established in Lemma 4.7. Consequently, it suffices to impose the condition

$$\varepsilon < \frac{1}{1 + 2^d},$$

which will be used repeatedly in the detailed proof. With such a choice of  $\varepsilon$ , we obtain the pointwise estimate

$$|g(\mathbf{x}) - Sg(\mathbf{x})| \leq (1 - \varepsilon) |g(\mathbf{x})| \quad \text{for all } \mathbf{x} \in [0, 1]^d,$$

yielding a uniform contraction of the residual. The remaining conclusions of Theorem 3.1, including strict  $L^p$  monotonicity and pointwise domination, emerge naturally from the preceding construction.

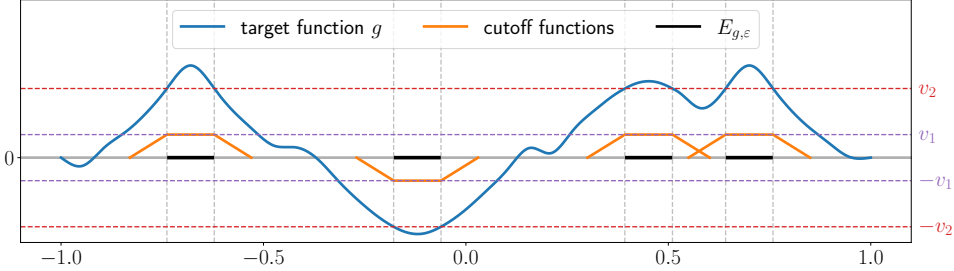


Figure 6: An illustration of cutoff functions associated with a target function  $g$ , where  $v_1 = \varepsilon \|g\|_{L^\infty([0,1]^d)}$  and  $v_2 = (1 - \varepsilon) \|g\|_{L^\infty([0,1]^d)}$ .

## 4.2 Preliminaries

We now present the technical preliminaries underlying the proof of Theorem 3.1. As outlined in Section 4.1, the proof follows a three-step strategy centered on constructing a suitable contraction mechanism. To formalize this approach, we first introduce the basic notions and structural assumptions on operators that will be used throughout the analysis, and establish several auxiliary definitions and lemmas that support the subsequent construction.

Throughout this section, we fix a domain  $\Omega \subseteq \mathbb{R}^n$  and a small parameter  $\varepsilon \in (0, 1)$ . All definitions and results below are formulated with respect to these standing assumptions. Our construction relies on separating the positive and negative contributions of a function and controlling them via suitable operators. For this reason, we begin by fixing notation for the positive and negative parts of a function.

**Definition 4.1.** For any real-valued function  $g$ , we write  $g = g^+ - g^-$ , where

$$g^+(\mathbf{x}) = \max\{g(\mathbf{x}), 0\} \quad \text{and} \quad g^-(\mathbf{x}) = \max\{-g(\mathbf{x}), 0\}.$$

The functions  $g^+$  and  $g^-$  denote the positive and negative parts of  $g$ , and this notation will be used throughout the paper.

We next introduce two notions of contractivity, which quantify the extent to which an operator drives a function toward its positive or balanced components.

**Definition 4.2.** An operator  $T : C(\Omega) \rightarrow C(\Omega)$  is called a *positive  $\varepsilon$ -contraction* if for any  $g \in C(\Omega)$ ,

$$\|g^+ - Tg\|_{L^\infty(\Omega)} \leq (1 - \varepsilon) \|g^+\|_{L^\infty(\Omega)}.$$

Similarly,  $T$  is called a *balanced  $\varepsilon$ -contraction* if for any  $g \in C(\Omega)$ ,

$$\|g - Tg\|_{L^\infty(\Omega)} \leq (1 - \varepsilon) \|g\|_{L^\infty(\Omega)}.$$

The positive  $\varepsilon$ -contraction controls only the positive part  $g^+$ , while the balanced  $\varepsilon$ -contraction acts on the full function  $g$ . In the proof of Theorem 3.1, we will first construct a positive contraction and then convert it into a balanced one by symmetrization.

To verify these contraction properties for a given operator, it is useful to isolate two basic structural conditions. The first provides a pointwise upper bound on  $Tg$ , expressed in terms of the positive part  $g^+$ . The second asserts that, whenever  $g$  is sufficiently close to the maximum of  $g^+$ , the operator  $T$  preserves a fixed proportion of this maximal value.

(C1) Pointwise bounds: for all  $g \in C(\Omega)$  and  $\mathbf{x} \in \Omega$ ,

$$0 \leq Tg(\mathbf{x}) \leq g^+(\mathbf{x}).$$

(C2) Stability near the maximum: for all  $g \in C(\Omega)$  and  $\mathbf{x} \in \Omega$ ,

$$g(\mathbf{x}) \geq (1 - \varepsilon) \|g^+\|_{L^\infty(\Omega)} \implies Tg(\mathbf{x}) \geq \varepsilon \|g^+\|_{L^\infty(\Omega)}.$$

Intuitively, condition (C1) enforces that  $T$  never overshoots the positive part of  $g$ , while condition (C2) guarantees that  $T$  retains a fixed fraction of the peak value whenever  $g$  is close to its maximum. Together, they are precisely tailored to yield a positive contraction in the sense defined above. The next lemma shows that these two simple structural conditions are already sufficient to imply a quantitative one-sided contraction.

**Lemma 4.3.** *Suppose that an operator  $T : C(\Omega) \rightarrow C(\Omega)$  satisfies conditions (C1) and (C2). Then  $T$  is a positive  $\varepsilon$ -contraction.*

*Proof.* Fix  $g \in C(\Omega)$  and define the level set

$$E_{g,\varepsilon} := \{\mathbf{x} \in \Omega : g(\mathbf{x}) \geq (1 - \varepsilon)\|g^+\|_{L^\infty(\Omega)}\}.$$

We consider separately the cases  $\mathbf{x} \in \Omega \setminus E_{g,\varepsilon}$  and  $\mathbf{x} \in E_{g,\varepsilon}$ .

**Case 1:**  $\mathbf{x} \in \Omega \setminus E_{g,\varepsilon}$ .

By definition of  $E_{g,\varepsilon}$  we have

$$g(\mathbf{x}) < (1 - \varepsilon)\|g^+\|_{L^\infty(\Omega)}.$$

In particular,

$$g^+(\mathbf{x}) = \max\{g(\mathbf{x}), 0\} \leq (1 - \varepsilon)\|g^+\|_{L^\infty(\Omega)}.$$

Using the pointwise bound (C1), we obtain

$$0 \leq Tg(\mathbf{x}) \leq g^+(\mathbf{x}),$$

and hence

$$0 \leq g^+(\mathbf{x}) - Tg(\mathbf{x}) \leq g^+(\mathbf{x}) \leq (1 - \varepsilon)\|g^+\|_{L^\infty(\Omega)}.$$

**Case 2:**  $\mathbf{x} \in E_{g,\varepsilon}$ .

In this case, the stability condition (C2) yields

$$Tg(\mathbf{x}) \geq \varepsilon\|g^+\|_{L^\infty(\Omega)}.$$

On the other hand, by (C1) we have  $Tg(\mathbf{x}) \leq g^+(\mathbf{x}) \leq \|g^+\|_{L^\infty(\Omega)}$ . Combining these two bounds, we obtain

$$0 \leq g^+(\mathbf{x}) - Tg(\mathbf{x}) \leq \|g^+\|_{L^\infty(\Omega)} - \varepsilon\|g^+\|_{L^\infty(\Omega)} = (1 - \varepsilon)\|g^+\|_{L^\infty(\Omega)}.$$

Combining the two cases, we conclude that for every  $\mathbf{x} \in \Omega$ ,

$$0 \leq g^+(\mathbf{x}) - Tg(\mathbf{x}) \leq (1 - \varepsilon)\|g^+\|_{L^\infty(\Omega)}.$$

Taking the supremum over  $\mathbf{x} \in \Omega$  gives

$$\|g^+ - Tg\|_{L^\infty(\Omega)} \leq (1 - \varepsilon)\|g^+\|_{L^\infty(\Omega)}.$$

This is precisely the positive  $\varepsilon$ -contraction estimate for  $T$  on the positive part of  $g$ .  $\square$

Having established a criterion for positive contractions, we now show how to extend such one-sided control to a fully balanced contraction via a standard symmetrization argument.

**Lemma 4.4.** *If  $T$  is a positive  $\varepsilon$ -contraction, then the symmetrized operator*

$$Sg := Tg - T(-g)$$

*is a balanced  $\varepsilon$ -contraction.*

*Proof.* Fix  $g \in C(\Omega)$  and decompose  $g = g^+ - g^-$  with  $g^+, g^- \geq 0$ . Note that

$$(-g)^+(\mathbf{x}) = \max\{-g(\mathbf{x}), 0\} = g^-(\mathbf{x}).$$

Applying the positive  $\varepsilon$ -contraction property to  $g$  and  $-g$  gives, for all  $\mathbf{x} \in \Omega$ ,

$$0 \leq g^+(\mathbf{x}) - Tg(\mathbf{x}) \leq (1 - \varepsilon)\|g^+\|_{L^\infty(\Omega)} \leq (1 - \varepsilon)\|g\|_{L^\infty(\Omega)},$$

and

$$0 \leq g^-(\mathbf{x}) - T(-g)(\mathbf{x}) \leq (1 - \varepsilon)\|g^-\|_{L^\infty(\Omega)} \leq (1 - \varepsilon)\|g\|_{L^\infty(\Omega)}.$$

By defining

$$a(\mathbf{x}) := g^+(\mathbf{x}) - Tg(\mathbf{x}) \quad \text{and} \quad b(\mathbf{x}) := g^-(\mathbf{x}) - T(-g)(\mathbf{x}).$$

we have

$$\begin{aligned} g(\mathbf{x}) - Sg(\mathbf{x}) &= (g^+(\mathbf{x}) - g^-(\mathbf{x})) - (Tg(\mathbf{x}) - T(-g)(\mathbf{x})) \\ &= (g^+(\mathbf{x}) - Tg(\mathbf{x})) - (g^-(\mathbf{x}) - T(-g)(\mathbf{x})) = a(\mathbf{x}) - b(\mathbf{x}). \end{aligned}$$

Since both  $a(\mathbf{x})$  and  $b(\mathbf{x})$  lie between 0 and  $(1 - \varepsilon)\|g\|_{L^\infty(\Omega)}$ , their difference satisfies

$$-(1 - \varepsilon)\|g\|_{L^\infty(\Omega)} \leq a(\mathbf{x}) - b(\mathbf{x}) \leq (1 - \varepsilon)\|g\|_{L^\infty(\Omega)}.$$

Hence, for all  $\mathbf{x} \in \Omega$ ,

$$|g(\mathbf{x}) - Sg(\mathbf{x})| \leq (1 - \varepsilon)\|g\|_{L^\infty(\Omega)},$$

which yields

$$\|g - Sg\|_{L^\infty(\Omega)} \leq (1 - \varepsilon)\|g\|_{L^\infty(\Omega)}.$$

Thus  $S$  is a balanced  $\varepsilon$ -contraction.  $\square$

Having established the structural framework and the overall contraction mechanism, we now turn to the concrete operator constructions used in our main theorem. To construct an operator satisfying conditions (C1) and (C2), we rely on a geometric decomposition of the domain into small hypercubes and associate to each cube a localized cutoff function. These cutoffs will later be implemented by shallow ReLU subnetworks.

**Definition 4.5** (Dilated hypercubes and continuous cutoff functions). Let  $Q \subseteq \mathbb{R}^d$  be a cube with center  $\mathbf{c}(Q)$  and side length  $\ell(Q)$ . For any  $r > 1$ , the  $r$ -dilate of  $Q$  is defined by

$$rQ := \{ \mathbf{c}(Q) + r(\mathbf{x} - \mathbf{c}(Q)) : \mathbf{x} \in Q \},$$

so that  $rQ$  is the cube concentric with  $Q$  and of side length  $r\ell(Q)$ .

A (continuous) cutoff function associated with  $Q$  is any map  $\Gamma_Q : \mathbb{R}^d \rightarrow [0, 1]$  satisfying

$$\Gamma_Q(\mathbf{x}) = 1 \text{ for } \mathbf{x} \in Q, \quad 0 \leq \Gamma_Q(\mathbf{x}) \leq 1 \text{ for } \mathbf{x} \in rQ \setminus Q, \quad \text{and} \quad \Gamma_Q(\mathbf{x}) = 0 \text{ for } \mathbf{x} \notin rQ.$$

Throughout this paper, we fix a dilation parameter  $r \in (1, 2)$ , for example  $r = \frac{3}{2}$ . To facilitate the implementation of cutoff functions using ReLU networks, we define  $\sigma(t) := \max\{t, 0\}$  and introduce the one-dimensional function

$$\psi(x) := \frac{1}{r-1}(\sigma(x+r) - \sigma(x+1) + \sigma(-x+r) - \sigma(-x+1)) - 1.$$

Figure 7 illustrates the function  $\psi$  for  $r = \frac{3}{2}$ . Based on  $\psi$ , we define the  $d$ -dimensional function

$$\Psi(\mathbf{x}) := \frac{1}{d} \sum_{i=1}^d \psi(x_i).$$

The cutoff function associated with  $Q$  is then defined by the rescaled map

$$\Gamma_Q(\mathbf{x}) := \Psi\left(\frac{2}{\ell(Q)}(\mathbf{x} - \mathbf{c}(Q))\right),$$

where  $\ell(Q)$  and  $\mathbf{c}(Q)$  denote the side length and center of  $Q$ , respectively.

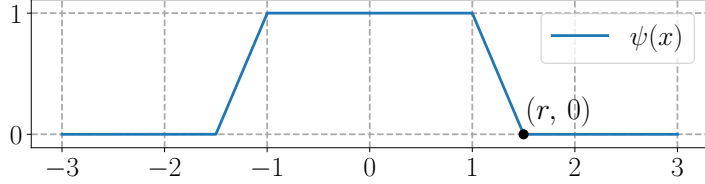


Figure 7: An illustration of  $\psi$ .

Below we present an explicit construction of an operator  $T_\varepsilon$  on  $C([0, 1]^d)$  that satisfies conditions (C1) and (C2) and therefore defines a positive  $\varepsilon$ -contraction. The construction is based on the dilated cube coverings and cutoff functions introduced above. Given  $\varepsilon \in (0, \frac{1}{1+2^d})$ , we define the operator  $T_\varepsilon : C([0, 1]^d) \rightarrow C([0, 1]^d)$  as follows. For any  $g \in C([0, 1]^d)$ , set

$$M_g := \|g^+\|_{L^\infty([0,1]^d)}.$$

If  $M_g = 0$ , we simply define  $T_\varepsilon g \equiv 0$ . In the nontrivial case  $M_g > 0$ , the construction proceeds in four steps below.

(i) Introduce the superlevel set

$$E_{g,\varepsilon} := \{\mathbf{x} \in [0, 1]^d : g(\mathbf{x}) \geq (1 - \varepsilon)M_g\}.$$

(ii) Define

$$\delta_{g,\varepsilon} := \sup \left\{ t \in (0, 1) : \omega_{g^+}(2\sqrt{d}t) \leq (1 - \varepsilon - 2^d\varepsilon)M_g \right\},$$

where the positive part  $g^+$  is used to ensure uniform control over regions in which  $g \geq 0$ . Here, for a general function  $f \in C([0, 1]^d)$ , the modulus of continuity  $\omega_f$  is defined by

$$\omega_f(t) := \sup \left\{ |f(\mathbf{x}) - f(\mathbf{y})| : \|\mathbf{x} - \mathbf{y}\|_2 \leq t, \mathbf{x}, \mathbf{y} \in [0, 1]^d \right\}, \quad t \geq 0.$$

We note that  $\varepsilon$  is chosen sufficiently small so that the factor  $1 - \varepsilon - 2^d\varepsilon$  remains positive. Since  $g^+ \in C([0, 1])^d$  and  $\omega_{g^+}(t) \rightarrow 0$  as  $t \rightarrow 0$ , the admissible set in the definition of  $\delta_{g,\varepsilon}$  is nonempty, and hence  $\delta_{g,\varepsilon} > 0$ .

(iii) Consider the uniform grid of cubes

$$\tilde{Q}_{g,\varepsilon,\beta} = \prod_{j=1}^d [\beta_j \delta_{g,\varepsilon}, (\beta_j + 1) \delta_{g,\varepsilon}], \quad \beta \in \mathbb{Z}^d,$$

which form a cover for  $\mathbb{R}^d$ . Since  $E_{g,\varepsilon} \subseteq [0, 1]^d$  is bounded, only finitely many such cubes intersect it. Let  $\{Q_{g,\varepsilon,i}\}_{i=1}^{n_{g,\varepsilon}}$  denote those cubes satisfying  $Q_{g,\varepsilon,i} \cap E_{g,\varepsilon} \neq \emptyset$ , so that

$$\bigcup_{i=1}^{n_{g,\varepsilon}} Q_{g,\varepsilon,i} \supseteq E_{g,\varepsilon}.$$

(iv) Define

$$T_\varepsilon g := \varepsilon M_g \sum_{i=1}^{n_{g,\varepsilon}} \Gamma_{Q_{g,\varepsilon,i}},$$

where  $\Gamma_{Q_{g,\varepsilon,i}}$  is the cutoff function associated with  $Q_{g,\varepsilon,i}$ , as introduced in Definition 4.5.

We remark that the operator  $T_\varepsilon$  constructed above satisfies the defining properties of a positive  $\varepsilon$ -contraction, as will be established in Lemma 4.9. Before proving this result, we introduce an auxiliary geometric lemma that plays a crucial role in controlling the overlap of the supports arising in the construction of  $T_\varepsilon$ .

*Remark 4.6.* The dilation factor  $r \in (1, 2)$  is introduced to balance two competing requirements. On the one hand, it ensures that any point sufficiently close to a cube intersecting  $E_{g,\varepsilon}$  lies within a uniformly bounded neighborhood, which is essential for deriving lower bounds on  $g$  via continuity estimates. On the other hand, restricting  $r < 2$  guarantees a uniform upper bound on the number of overlapping dilated cubes at any point. This balance is fundamental to establishing both the positivity and the contractivity properties of  $T_\varepsilon$ .

**Lemma 4.7** (Bounded overlap under small centered dilation). *Let  $\delta > 0$  and consider the axis-aligned grid of cubes*

$$Q_\beta := \prod_{j=1}^d [\beta_j \delta, (\beta_j + 1)\delta], \quad \beta \in \mathbb{Z}^d.$$

*Then, for any  $r \in (1, 2)$  and every  $\mathbf{x} \in \mathbb{R}^d$ ,*

$$|\{\beta \in \mathbb{Z}^d : \mathbf{x} \in rQ_\beta\}| \leq 2^d.$$

*Proof.* Each cube can be written in centered form as

$$Q_\beta = \mathbf{c}_\beta + \left[ -\frac{\delta}{2}, \frac{\delta}{2} \right]^d, \quad \mathbf{c}_\beta := \delta(\beta + \frac{1}{2}\mathbf{1}), \quad \beta \in \mathbb{Z}^d.$$

Fix  $\mathbf{x} \in \mathbb{R}^d$ . The condition  $\mathbf{x} \in rQ_\beta$  is equivalent, coordinatewise, to

$$|x_j - c_{\beta,j}| \leq \frac{r\delta}{2}, \quad j = 1, 2, \dots, d.$$

Substituting  $c_{\beta,j} := \delta(\beta_j + \frac{1}{2})$ , this inequality becomes

$$\left| \frac{x_j}{\delta} - (\beta_j + \frac{1}{2}) \right| \leq \frac{r}{2}.$$

Thus, for each coordinate  $j$ , the index  $\beta_j$  must lie in an interval of length  $r < 2$  on the real line. Any interval of length strictly less than 2 contains at most two integers, and hence there are at most two admissible values of  $\beta_j$  for each coordinate.

Since the coordinates are independent, the total number of multi-indices  $\beta := (\beta_1, \dots, \beta_d)$  satisfying  $\mathbf{x} \in rQ_\beta$  is bounded above by  $2^d$ .  $\square$

*Remark 4.8.* The bound in Lemma 4.7 is sharp. when  $\mathbf{x}$  is a vertex of the grid, exactly  $2^d$  dilated cubes contain  $\mathbf{x}$  for any  $r > 1$ . The overlap can exceed  $2^d$  only when  $r\delta/2 \geq \delta$ , that is, when  $r \geq 2$ , corresponding to a dilation that at least doubles the side length of the cubes.

With Lemma 4.7 in hand, we are prepared to verify that the operator  $T_\varepsilon$  satisfies conditions (C1) and (C2). By Lemma 4.3, these two conditions together imply that  $T_\varepsilon$  is a positive  $\varepsilon$ -contraction, as stated in Lemma 4.9 below.

**Lemma 4.9.** *Let  $T_\varepsilon$  be the operator defined above. Then  $T_\varepsilon$  satisfies conditions (C1) and (C2). Consequently,  $T_\varepsilon$  is a positive  $\varepsilon$ -contraction.*

*Proof.* We verify conditions (C1) and (C2).

**Verification of condition (C1).**

By the construction of  $T_\varepsilon$ ,

$$T_\varepsilon g(\mathbf{x}) = \varepsilon M_g \sum_{i=1}^{n_{g,\varepsilon}} \Gamma_{Q_{g,\varepsilon,i}}(\mathbf{x}) \geq 0,$$

since each cutoff function is nonnegative. We may assume  $M_g > 0$ , as the case  $M_g = 0$  implies  $T_\varepsilon g \equiv 0$  and is trivial.

Fix any

$$\mathbf{x} \in A_{g,\varepsilon} := \left( \bigcup_{i=1}^{n_{g,\varepsilon}} rQ_{g,\varepsilon,i} \right) \cap [0, 1]^d, \quad r \in (1, 2).$$

By Lemma 4.7, the point  $\mathbf{x}$  belongs to at most  $2^d$  dilated cubes. Therefore,

$$0 \leq \sum_{i=1}^{n_{g,\varepsilon}} \Gamma_{Q_{g,\varepsilon,i}}(\mathbf{x}) \leq 2^d,$$

which yields

$$0 \leq T_\varepsilon g(\mathbf{x}) \leq 2^d \varepsilon M_g, \quad \mathbf{x} \in A_{g,\varepsilon}. \quad (1)$$

Now choose an index  $i$  such that  $\mathbf{x} \in rQ_{g,\varepsilon,i}$ . Since  $Q_{g,\varepsilon,i} \cap E_{g,\varepsilon} \neq \emptyset$  by construction, there exists  $\tilde{\mathbf{x}} \in Q_{g,\varepsilon,i} \cap E_{g,\varepsilon}$ . Because both  $\mathbf{x}$  and  $\tilde{\mathbf{x}}$  lie in the same dilated cube  $rQ_{g,\varepsilon,i}$ ,

$$\|\mathbf{x} - \tilde{\mathbf{x}}\|_2 \leq r\sqrt{d} \delta_{g,\varepsilon} \leq 2\sqrt{d} \delta_{g,\varepsilon}.$$

Recall that

$$E_{g,\varepsilon} = \{\mathbf{x} : g(\mathbf{x}) \geq (1 - \varepsilon)M_g\}$$

and the definition of  $\delta_{g,\varepsilon}$ , we obtain

$$\begin{aligned} g(\mathbf{x}) &\geq g(\tilde{\mathbf{x}}) - \omega_{g+}(2\sqrt{d} \delta_{g,\varepsilon}) \\ &\geq (1 - \varepsilon)M_g - (1 - \varepsilon - 2^d \varepsilon)M_g = 2^d \varepsilon M_g. \end{aligned}$$

Thus,

$$2^d \varepsilon M_g \leq g(\mathbf{x}) \leq M_g, \quad \mathbf{x} \in A_{g,\varepsilon}. \quad (2)$$

If instead

$$\mathbf{x} \notin \bigcup_{i=1}^{n_{g,\varepsilon}} rQ_{g,\varepsilon,i},$$

then  $\Gamma_{Q_{g,\varepsilon,i}}(\mathbf{x}) = 0$  for all  $i$ , and hence

$$T_\varepsilon g(\mathbf{x}) = 0. \quad (3)$$

Combining (1), (2), and (3), we conclude that

$$0 \leq T_\varepsilon g(\mathbf{x}) \leq g^+(\mathbf{x}) \quad \text{for all } \mathbf{x} \in [0, 1]^d,$$

which establishes condition (C1).

### Verification of condition (C2).

Let  $\mathbf{x} \in [0, 1]^d$  satisfy  $g(\mathbf{x}) \geq (1 - \varepsilon)M_g$ . Then  $\mathbf{x} \in E_{g,\varepsilon}$  and hence belongs to some cube  $Q_{g,\varepsilon,i}$ . By definition of the cutoff function,  $\Gamma_{Q_{g,\varepsilon,i}}(\mathbf{x}) = 1$ . Therefore,

$$T_\varepsilon g(\mathbf{x}) = \varepsilon M_g \sum_{i=1}^{n_{g,\varepsilon}} \Gamma_{Q_{g,\varepsilon,i}}(\mathbf{x}) \geq \varepsilon M_g,$$

which verifies condition (C2).

Both conditions are satisfied, and hence  $T_\varepsilon$  is a positive  $\varepsilon$ -contraction.  $\square$

### 4.3 Main argument

We now assemble the components developed above. The operator  $T_\varepsilon$  provides a one-sided contraction on the positive part of a continuous function, while its symmetrization  $S_\varepsilon$  yields a balanced  $\varepsilon$ -contraction on the entire function. We now show that  $S_\varepsilon$  can be realized by a finite multigrade ReLU architecture, thereby proving Theorem 3.1.

*Proof of Theorem 3.1.* The proof proceeds in two stages.

#### Stage I: Network realization of the contraction.

Let  $T_\varepsilon$  be the operator constructed in the previous section. Throughout the proof, we apply  $T_\varepsilon$  to both  $f$  and  $-f$ ; hence all quantities

$$M_g, \quad \Gamma_{Q_{g,\varepsilon,i}}, \quad n_{g,\varepsilon}$$

are understood with  $g = f$  or  $g = -f$ .

By definition, for  $\mathbf{x} \in [0, 1]^d$ ,

$$T_\varepsilon f(\mathbf{x}) = \varepsilon M_f \sum_{i=1}^{n_{f,\varepsilon}} \Gamma_{Q_{f,\varepsilon,i}}(\mathbf{x}),$$

and likewise,

$$T_\varepsilon(-f)(\mathbf{x}) = \varepsilon M_{-f} \sum_{i=1}^{n_{-f,\varepsilon}} \Gamma_{Q_{-f,\varepsilon,i}}(\mathbf{x}).$$

By Lemma 4.9,  $T_\varepsilon$  is a positive  $\varepsilon$ -contraction, and Lemma 4.4 implies that the symmetrized operator

$$S_\varepsilon f := T_\varepsilon f - T_\varepsilon(-f)$$

is a balanced  $\varepsilon$ -contraction.

For notational convenience, define

$$n := n_{f,\varepsilon} + n_{-f,\varepsilon},$$

and introduce unified sequence  $\{\widehat{M}_k\}_{k=1}^n$  by

$$\widehat{M}_k := \begin{cases} M_f, & k = 1, \dots, n_{f,\varepsilon}, \\ -M_{-f}, & k = n_{f,\varepsilon} + 1, \dots, n, \end{cases}$$

and  $\{\widehat{Q}_k\}_{k=1}^n$  by

$$\widehat{Q}_k := \begin{cases} Q_{f,\varepsilon,k}, & k = 1, \dots, n_{f,\varepsilon}, \\ Q_{-f,\varepsilon,k-n_{f,\varepsilon}}, & k = n_{f,\varepsilon} + 1, \dots, n. \end{cases}$$

Then

$$S_\varepsilon f = \sum_{k=1}^n h_k, \quad \text{where } h_k := \varepsilon \widehat{M}_k \Gamma_{\widehat{Q}_k}.$$

We remark that, according to the definition of  $T_\varepsilon$ , the value of  $n$  depends primarily on the modulus of continuity  $\omega_f$  (which reflects the complexity of the target function  $f$ ) and the prescribed  $\varepsilon$ .

Let  $\ell_k$  and  $\mathbf{c}_k$  denote the side length and center of  $\widehat{Q}_k$ . By Definition 4.5,

$$\Gamma_{\widehat{Q}_k}(\mathbf{x}) = \Psi\left(\frac{2}{\ell_k}(\mathbf{x} - \mathbf{c}_k)\right),$$

where  $\Psi$  is constructed from one-dimensional ReLU combinations. As illustrated in Figure 8, there exist affine maps

$$\mathcal{A}_k, \mathcal{A}_k^{\text{out}} \in \text{Aff}_{\leq 5d}, \quad k = 1, 2, \dots, n,$$

such that

$$h_k = \mathcal{A}_k^{\text{out}} \circ (\text{ReLU} \circ \mathcal{A}_k) \circ \dots \circ (\text{ReLU} \circ \mathcal{A}_1).$$

Consequently, the entire operator  $S_\varepsilon$  is realized by a residual ReLU network of width  $5d$  and depth  $n$ , with each grade contributing one update block, as required in Theorem 3.1.

### Stage II: Decay of the residual.

Define  $f_1 = f$  and recursively

$$f_{k+1} = f_k - h_k, \quad k = 1, \dots, n.$$

By construction,

$$f_{n+1} = f - \sum_{k=1}^n h_k = f - S_\varepsilon f.$$

Since  $S_\varepsilon$  is a balanced  $\varepsilon$ -contraction,

$$\|f_{n+1}\|_{L^\infty([0,1]^d)} = \|f - S_\varepsilon f\|_{L^\infty([0,1]^d)} \leq (1 - \varepsilon) \|f\|_{L^\infty([0,1]^d)}.$$

We now show that each update produces pointwise monotone decay and a strict decrease in  $L^p$  norms. By Lemma 4.9,

$$0 \leq T_\varepsilon f(\mathbf{x}) \leq f^+(\mathbf{x}), \quad 0 \leq T_\varepsilon(-f)(\mathbf{x}) \leq f^-(\mathbf{x}),$$

which implies

$$\sum_{k=1}^{n_{f,\varepsilon}} h_k(\mathbf{x}) \leq f^+(\mathbf{x}), \quad - \sum_{k=n_{f,\varepsilon}+1}^n h_k(\mathbf{x}) \leq f^-(\mathbf{x}). \quad (4)$$

Let

$$\Omega_1 := \{\mathbf{x} \in [0, 1]^d : f(\mathbf{x}) \geq 0\}, \quad \Omega_2 := \{\mathbf{x} \in [0, 1]^d : f(\mathbf{x}) < 0\}$$

and observe that  $[0, 1]^d = \Omega_1 \cup \Omega_2$ .

*Case 1:  $k \leq n_{f,\varepsilon}$  (positive-side update).*

We first consider the pointwise estimate. For  $\mathbf{x} \in \Omega_1$ , by (4),

$$f_{k+1}(\mathbf{x}) = f(\mathbf{x}) - \sum_{j=1}^k h_j(\mathbf{x}) = f^+(\mathbf{x}) - \sum_{j=1}^k h_j(\mathbf{x}) \geq 0.$$

Moreover, we have  $h_k(\mathbf{x}) = \varepsilon M_f \Gamma_{\hat{Q}_k}(\mathbf{x}) \geq 0$  for  $\mathbf{x} \in \Omega_1$  and hence

$$0 \leq f_{k+1}(\mathbf{x}) = f_k(\mathbf{x}) - h_k(\mathbf{x}) \leq f_k(\mathbf{x}).$$

For  $\mathbf{x} \in \Omega_2$ ,  $h_k(\mathbf{x}) = 0$ , so  $f_{k+1}(\mathbf{x}) = f_k(\mathbf{x})$ . Thus

$$|f_{k+1}(\mathbf{x})| \leq |f_k(\mathbf{x})|, \quad \mathbf{x} \in \Omega_1 \cup \Omega_2 = [0, 1]^d.$$

We next consider the  $L^p$  norm estimate for  $p \in [1, \infty)$ . Since  $f_k(\mathbf{x}) \geq h_k(\mathbf{x}) \geq 0$  for all  $\mathbf{x} \in \Omega_1$ , and that  $h_k(\mathbf{x}) > 0$  on the cube  $\hat{Q}_k \subseteq \Omega_1$ ,

$$\int_{\Omega_1} |f_{k+1}(\mathbf{x})|^p d\mathbf{x} = \int_{\Omega_1} |f_k(\mathbf{x}) - h_k(\mathbf{x})|^p d\mathbf{x} < \int_{\Omega_1} |f_k(\mathbf{x})|^p d\mathbf{x}.$$

Moreover

$$\int_{\Omega_2} |f_{k+1}(\mathbf{x})|^p d\mathbf{x} = \int_{\Omega_2} |f_k(\mathbf{x}) - h_k(\mathbf{x})|^p d\mathbf{x} = \int_{\Omega_2} |f_k(\mathbf{x})|^p d\mathbf{x}$$

Therefore,

$$\|f_{k+1}\|_{L^p([0,1]^d)} < \|f_k\|_{L^p([0,1]^d)}.$$

Case 2:  $k > n_{f,\varepsilon}$  (negative-side update).

We first consider the pointwise estimate. For  $\mathbf{x} \in \Omega_2$ , we have  $f^+(\mathbf{x}) = 0$ , implying

$$h_j(\mathbf{x}) = 0, \quad j \leq n_{f,\varepsilon}.$$

Then by (4),

$$f_{k+1}(\mathbf{x}) = f(\mathbf{x}) - \sum_{j=1}^k h_j(\mathbf{x}) = -f^-(\mathbf{x}) - \sum_{j=n_{f,\varepsilon}+1}^k h_j(\mathbf{x}) \leq 0.$$

Moreover,

$$h_k(\mathbf{x}) = -\varepsilon M_{-f} \Gamma_{\widehat{Q}_k}(\mathbf{x}) \leq 0, \quad \mathbf{x} \in \Omega_2,$$

from which we deduce

$$0 \geq f_{k+1}(\mathbf{x}) = f_k(\mathbf{x}) - h_k(\mathbf{x}) \geq f_k(\mathbf{x}), \quad \mathbf{x} \in \Omega_2.$$

For  $\mathbf{x} \in \Omega_1$ , we have  $h_k(\mathbf{x}) = 0$ , and hence

$$f_{k+1}(\mathbf{x}) = f_k(\mathbf{x}) - h_k(\mathbf{x}) = f_k(\mathbf{x}).$$

Consequently,

$$|f_{k+1}(\mathbf{x})| \leq |f_k(\mathbf{x})|, \quad \mathbf{x} \in \Omega_1 \cup \Omega_2 = [0, 1]^d.$$

We next consider the  $L^p$  norm estimate for  $p \in [1, \infty)$ . Clearly,

$$\int_{\Omega_2} |f_{k+1}(\mathbf{x})|^p d\mathbf{x} = \int_{\Omega_2} |f_k(\mathbf{x}) - h_k(\mathbf{x})|^p d\mathbf{x} < \int_{\Omega_2} |f_k(\mathbf{x})|^p d\mathbf{x}.$$

The strict inequality follows from the facts that  $f_k(\mathbf{x}) \leq h_k(\mathbf{x}) \leq 0$  for all  $\mathbf{x} \in \Omega_2$ , and that  $h_k(\mathbf{x}) < 0$  on the set  $\widehat{Q}_k \subseteq \Omega_2$ . Moreover

$$\int_{\Omega_1} |f_{k+1}(\mathbf{x})|^p d\mathbf{x} = \int_{\Omega_1} |f_k(\mathbf{x}) - h_k(\mathbf{x})|^p d\mathbf{x} = \int_{\Omega_1} |f_k(\mathbf{x})|^p d\mathbf{x}$$

Therefore,

$$\|f_{k+1}\|_{L^p([0,1]^d)} < \|f_k\|_{L^p([0,1]^d)}.$$

Combining both cases, for  $k = 1, 2, \dots, n$ , we have

$$|f_{k+1}(\mathbf{x})| \leq |f_k(\mathbf{x})|, \quad \mathbf{x} \in [0, 1]^d,$$

and for every  $1 \leq p < \infty$ ,

$$\|f_{k+1}\|_{L^p([0,1]^d)} < \|f_k\|_{L^p([0,1]^d)},$$

which completes the proof.  $\square$

To close this section, we illustrate the architecture that realizes  $\Psi_k$  in the proof of Theorem 3.1. As depicted in Figure 8, there exist affine maps  $\mathcal{A}_k, \mathcal{A}_k^{\text{out}} \in \text{Aff}_{\leq 5d}$  for  $k = 1, 2, \dots, n$  such that each  $h_k$  admits a representation of the form

$$h_k = \mathcal{A}_k^{\text{out}} \circ (\text{ReLU} \circ \mathcal{A}_k) \circ \dots \circ (\text{ReLU} \circ \mathcal{A}_1).$$

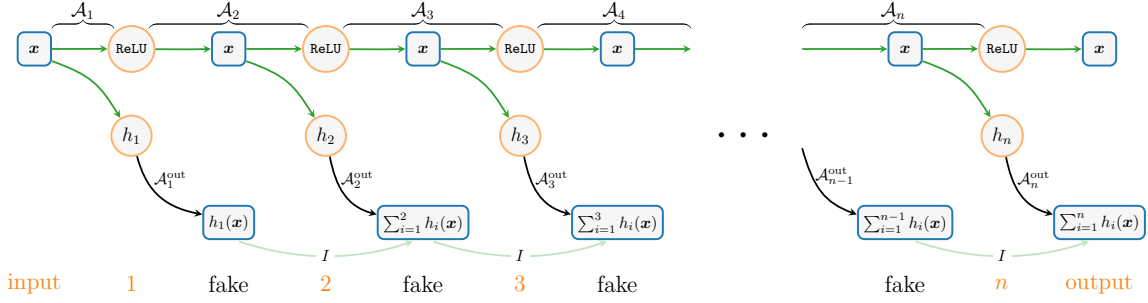


Figure 8: An illustration of the network architecture used to realize  $h_k$  for  $\mathbf{x} \in [0, 1]^d$ .

We remark that the circled symbols  $\text{ReLU}$  and  $h_k$  in Figure 8 are mildly schematic. The circled  $\text{ReLU}$  represents a block of  $d$   $\text{ReLU}$  units, while the circled  $\Psi_k$  corresponds to  $4d$   $\text{ReLU}$  units. Thus the entire architecture in Figure 8 may be viewed as a residual  $\text{ReLU}$  network of width  $5d$  and depth  $n$ , with  $I$  denoting the identity map. The affine map  $\mathcal{A}_k^{\text{out}}$  is represented by the black arrow and provides the final scaling needed to produce  $\Psi_k$ . Each intermediate map  $\mathcal{A}_i$  arises from composing the affine transformations that appear immediately before and after the corresponding ‘fake layer’ in the diagram. This fake layer is not an actual network layer, since it contains no activation; it serves solely to separate successive affine maps and to clarify the theoretical decomposition of  $h_k$  in the diagram. In particular, summing these grade-wise updates yields exactly the recursive structure required in Theorem 3.1, with each update realized by a width- $5d$   $\text{ReLU}$  network block followed by an affine output map.

## 5 Conclusion

In this work, we establish a rigorous theoretical foundation for MGDL as a structured error refinement framework within function approximation theory. By formulating the grade-wise training process in operator-theoretic terms, we identify explicit structural conditions under which a fixed-width multigrade  $\text{ReLU}$  architecture achieves strict residual contraction at every grade and converges uniformly to the target function. These results provide a constructive and transparent explanation of how approximation accuracy can be progressively enhanced with depth through controlled, hierarchical residual updates.

Our analysis positions MGDL as a principled alternative to conventional end-to-end training. Rather than optimizing all layers simultaneously, MGDL resolves approximation error via a sequence of monotone refinements, thereby reducing adverse nonconvex interactions and elucidating the functional role of depth in deep neural networks. The resulting theoretical guarantees not only complement existing empirical observations but also connect MGDL to classical concepts in approximation theory and hierarchical modeling.

Several directions for future research naturally follow from this work. A primary extension is to broaden the analysis beyond fixed-width  $\text{ReLU}$  networks to encompass other activation functions and architectural families. Another open problem concerns the optimization landscape of practical MGDL implementations, in which network parameters are learned from data rather than constructed analytically, and how such training dynamics affect stability and generalization. Finally, integrating multigrade principles into modern architectures, including transformers, neural operators, and physics-informed models, offers a promising pathway toward scalable learning systems that unify theoretical guarantees with practical effectiveness.

## Acknowledgments

Shijun Zhang was partially supported by the start-up fund P0053092 from The Hong Kong Polytechnic University. Zuowei Shen was partially supported under the Distinguished Profes-

sorship of National University of Singapore. Yuesheng Xu was supported in part by the US National Science Foundation under Grant DMS-2208386.

## References

- [1] Sanjeev Arora, Zhiyuan Li, and Abhishek Panigrahi. Understanding gradient descent on the edge of stability in deep learning. In *International Conference on Machine Learning*, pages 948–1024. PMLR, 2022.
- [2] Chenglong Bao, Qianxiao Li, Zuowei Shen, Cheng Tai, Lei Wu, and Xueshuang Xiang. Approximation analysis of convolutional neural networks. *East Asian Journal on Applied Mathematics*, 13(3):524–549, 2023. URL: [http://global-sci.org/intro/article\\_detail/eajam/21721.html](http://global-sci.org/intro/article_detail/eajam/21721.html), doi:10.4208/eajam.2022-270.070123.
- [3] Ronen Basri, Meirav Galun, Amnon Geifman, David Jacobs, Yoni Kasten, and Shira Kritchman. Frequency bias in neural networks for input of non-uniform density. In Hal Daumé III and Aarti Singh, editors, *Proceedings of the 37th International Conference on Machine Learning*, volume 119 of *Proceedings of Machine Learning Research*, pages 685–694. PMLR, 13–18 Jul 2020. URL: <https://proceedings.mlr.press/v119/basri20a.html>.
- [4] Yoshua Bengio, Pascal Lamblin, Dan Popovici, and Hugo Larochelle. Greedy layer-wise training of deep networks. In *Proceedings of the 20th International Conference on Neural Information Processing Systems*, NIPS’06, page 153–160, Cambridge, MA, USA, 2006. MIT Press.
- [5] Helmut. Bölcskei, Philipp. Grohs, Gitta. Kutyniok, and Philipp. Petersen. Optimal approximation with sparsely connected deep neural networks. *SIAM Journal on Mathematics of Data Science*, 1(1):8–45, 2019. arXiv:<https://doi.org/10.1137/18M118709X>, doi:10.1137/18M118709X.
- [6] Jeremy M Cohen, Simran Kaur, Yuanzhi Li, J Zico Kolter, and Ameet Talwalkar. Gradient descent on neural networks typically occurs at the edge of stability. *arXiv preprint arXiv:2103.00065*, 2021.
- [7] George Cybenko. Approximation by superpositions of a sigmoidal function. *Mathematics of Control, Signals, and Systems*, 2:303–314, 1989. doi:10.1007/BF02551274.
- [8] Shizhe Ding, Boyang Xia, and Dongbo Bu. Accurate interpolation for scattered data through hierarchical residual refinement. In A. Oh, T. Naumann, A. Globerson, K. Saenko, M. Hardt, and S. Levine, editors, *Advances in Neural Information Processing Systems*, volume 36, pages 9144–9155. Curran Associates, Inc., 2023. URL: [https://proceedings.neurips.cc/paper\\_files/paper/2023/file/1d5a92867cf463fad136cfa23395840b-Paper-Conference.pdf](https://proceedings.neurips.cc/paper_files/paper/2023/file/1d5a92867cf463fad136cfa23395840b-Paper-Conference.pdf).
- [9] Feng-Lei Fan, Dayang Wang, Hengtao Guo, Qikui Zhu, Pingkun Yan, Ge Wang, and Hengyong Yu. On a sparse shortcut topology of artificial neural networks. *IEEE Transactions on Artificial Intelligence*, 3(4):595–608, 2022. doi:10.1109/TAI.2021.3128132.
- [10] Ronglong Fang and Yuesheng Xu. Addressing spectral bias of deep neural networks by multi-grade deep learning. *Advances in Neural Information Processing Systems 37*, 2024.
- [11] Ronglong Fang and Yuesheng Xu. Computational advantages of multi-grade deep learning: Convergence analysis and performance insights. *arXiv preprint*, 2025. arXiv:2507.20351.

- [12] Rémi Gribonval, Gitta Kutyniok, Morten Nielsen, and Felix Voigtlaender. Approximation spaces of deep neural networks. *Constructive Approximation*, 55:259–367, 2022. doi: 10.1007/s00365-021-09543-4.
- [13] Ingo Gühring, Gitta Kutyniok, and Philipp Petersen. Error bounds for approximations with deep ReLU neural networks in  $W^{s,p}$  norms. *Analysis and Applications*, 18(05):803–859, 2020. arXiv:<https://doi.org/10.1142/S0219530519410021>, doi:10.1142/S0219530519410021.
- [14] Kaiming He, Xiangyu Zhang, Shaoqing Ren, and Jian Sun. Deep Residual Learning for Image Recognition . In *2016 IEEE Conference on Computer Vision and Pattern Recognition (CVPR)*, pages 770–778, Los Alamitos, CA, USA, June 2016. IEEE Computer Society. URL: <https://doi.ieee.org/10.1109/CVPR.2016.90>, doi:10.1109/CVPR.2016.90.
- [15] Geoffrey E. Hinton, Simon Osindero, and Yee-Whye Teh. A fast learning algorithm for deep belief nets. *Neural Computation*, 18(7):1527–1554, 2006. doi:10.1162/neco.2006.18.7.1527.
- [16] Kurt Hornik. Approximation capabilities of multilayer feedforward networks. *Neural Networks*, 4(2):251–257, 1991. URL: <http://www.sciencedirect.com/science/article/pii/089360809190009T>, doi:10.1016/0893-6080(91)90009-T.
- [17] Kurt Hornik, Maxwell Stinchcombe, and Halbert White. Multilayer feedforward networks are universal approximators. *Neural Networks*, 2(5):359–366, 1989. URL: <http://www.sciencedirect.com/science/article/pii/0893608089900208>, doi:10.1016/0893-6080(89)90020-8.
- [18] Jie Jiang and Yuesheng Xu. Deep neural network solutions for oscillatory fredholm integral equations. *Journal of Integral Equations and Applications*, 36 (1), 2024.
- [19] Jie Jiang and Yuesheng Xu. Adaptive multi-grade deep learning for highly oscillatory fredholm integral equations of the second kind. *Journal of Scientific Computing*, accepted, 2026, arXiv preprint arXiv:2601.04496.
- [20] Diederik P. Kingma and Jimmy Ba. Adam: A method for stochastic optimization. In Yoshua Bengio and Yann LeCun, editors, *3rd International Conference on Learning Representations, ICLR 2015, San Diego, CA, USA, May 7-9, 2015, Conference Track Proceedings*, 2015. URL: <http://arxiv.org/abs/1412.6980>.
- [21] Qianxiao Li, Ting Lin, and Zuowei Shen. Deep learning via dynamical systems: An approximation perspective. *Journal of the European Mathematical Society*, 25(5):1671–1709, 2023. doi:10.4171/JEMS/1221.
- [22] Jianfeng Lu, Zuowei Shen, Haizhao Yang, and Shijun Zhang. Deep network approximation for smooth functions. *SIAM Journal on Mathematical Analysis*, 53(5):5465–5506, 2021. doi:10.1137/20M134695X.
- [23] Tao Luo, Zheng Ma, Zhi-Qin John Xu, and Yaoyu Zhang. Theory of the frequency principle for general deep neural networks. *CSIAM Transactions on Applied Mathematics*, 2(3):484–507, 2021. URL: [http://global-sci.org/intro/article\\_detail/csiam-am/19447.html](http://global-sci.org/intro/article_detail/csiam-am/19447.html), doi:10.4208/csiam-am.S0-2020-0005.
- [24] Hadrien Montanelli and Haizhao Yang. Error bounds for deep ReLU networks using the Kolmogorov-Arnold superposition theorem. *Neural Networks*, 129:1–6, 2020. URL: <http://www.sciencedirect.com/science/article/pii/S0893608019304058>, doi:10.1016/j.neunet.2019.12.013.

[25] Boris Oreshkin, Dmytro Carpov, Nicolas Chapados, and Yoshua Bengio. N-beats: Neural basis expansion analysis for time series forecasting. In *International Conference on Learning Representations (ICLR)*, 2020.

[26] Mert Pilanci and Tolga Ergen. Neural networks are convex regularizers: Exact polynomial-time convex optimization formulations for two-layer networks. In Hal Daumé III and Aarti Singh, editors, *Proceedings of the 37th International Conference on Machine Learning*, volume 119 of *Proceedings of Machine Learning Research*, pages 7695–7705. PMLR, 13–18 Jul 2020. URL: <https://proceedings.mlr.press/v119/pilanci20a.html>.

[27] Nasim Rahaman, Aristide Baratin, Devansh Arpit, Felix Draxler, Min Lin, Fred Hamprecht, Yoshua Bengio, and Aaron Courville. On the spectral bias of neural networks. In *International conference on machine learning*, pages 5301–5310. PMLR, 2019.

[28] Nasim Rahaman, Aristide Baratin, Devansh Arpit, Felix Draxler, Min Lin, Fred Hamprecht, Yoshua Bengio, and Aaron Courville. On the spectral bias of neural networks. In Kamalika Chaudhuri and Ruslan Salakhutdinov, editors, *Proceedings of the 36th International Conference on Machine Learning*, volume 97 of *Proceedings of Machine Learning Research*, pages 5301–5310. PMLR, 09–15 Jun 2019. URL: <https://proceedings.mlr.press/v97/rahaman19a.html>.

[29] Amos Ron and Zuowei Shen. Affine systems in  $L^2(\mathbb{R}^d)$ : The analysis of the analysis operator. *Journal of Functional Analysis*, 148(2):408–447, 1997. URL: <https://www.sciencedirect.com/science/article/pii/S0022123696930797>, doi:10.1006/jfan.1996.3079.

[30] Itay Safran and Ohad Shamir. Spurious local minima are common in two-layer ReLU neural networks. In Jennifer Dy and Andreas Krause, editors, *Proceedings of the 35th International Conference on Machine Learning*, volume 80 of *Proceedings of Machine Learning Research*, pages 4433–4441. PMLR, 10–15 Jul 2018. URL: <https://proceedings.mlr.press/v80/safran18a.html>.

[31] Shai Shalev-Shwartz, Ohad Shamir, and Shaked Shammah. Failures of gradient-based deep learning. In Doina Precup and Yee Whye Teh, editors, *Proceedings of the 34th International Conference on Machine Learning*, volume 70 of *Proceedings of Machine Learning Research*, pages 3067–3075. PMLR, 06–11 Aug 2017. URL: <https://proceedings.mlr.press/v70/shalev-shwartz17a.html>.

[32] Zuowei Shen, Haizhao Yang, and Shijun Zhang. Deep network approximation characterized by number of neurons. *Communications in Computational Physics*, 28(5):1768–1811, 2020. doi:10.4208/cicp.OA-2020-0149.

[33] Zuowei Shen, Haizhao Yang, and Shijun Zhang. Deep network with approximation error being reciprocal of width to power of square root of depth. *Neural Computation*, 33(4):1005–1036, 03 2021. URL: [https://doi.org/10.1162/neco\\_a\\_01364](https://doi.org/10.1162/neco_a_01364), arXiv:[https://direct.mit.edu/neco/article-pdf/33/4/1005/1900052/neco\\_a\\_01364.pdf](https://direct.mit.edu/neco/article-pdf/33/4/1005/1900052/neco_a_01364.pdf), doi:10.1162/neco\_a\_01364.

[34] Zuowei Shen, Haizhao Yang, and Shijun Zhang. Neural network approximation: Three hidden layers are enough. *Neural Networks*, 141:160–173, 2021. doi:10.1016/j.neunet.2021.04.011.

[35] Zuowei Shen, Haizhao Yang, and Shijun Zhang. Deep network approximation: Achieving arbitrary accuracy with fixed number of neurons. *Journal of Machine Learning Research*, 23(276):1–60, 2022. URL: <http://jmlr.org/papers/v23/21-1404.html>.

[36] Zuowei Shen, Haizhao Yang, and Shijun Zhang. Deep network approximation in terms of intrinsic parameters. In Kamalika Chaudhuri, Stefanie Jegelka, Le Song, Csaba Szepesvari, Gang Niu, and Sivan Sabato, editors, *Proceedings of the 39th International Conference on Machine Learning*, volume 162 of *Proceedings of Machine Learning Research*, pages 19909–19934. PMLR, 17–23 Jul 2022. URL: <https://proceedings.mlr.press/v162/shen22g.html>.

[37] Zuowei Shen, Haizhao Yang, and Shijun Zhang. Neural network architecture beyond width and depth. In S. Koyejo, S. Mohamed, A. Agarwal, D. Belgrave, K. Cho, and A. Oh, editors, *Advances in Neural Information Processing Systems*, volume 35, pages 5669–5681. Curran Associates, Inc., 2022. URL: [https://proceedings.neurips.cc/paper\\_files/paper/2022/hash/257be12f31dfa7cc158dda99822c6fd1-Abstract-Conference.html](https://proceedings.neurips.cc/paper_files/paper/2022/hash/257be12f31dfa7cc158dda99822c6fd1-Abstract-Conference.html).

[38] Zuowei Shen, Haizhao Yang, and Shijun Zhang. Optimal approximation rate of ReLU networks in terms of width and depth. *Journal de Mathématiques Pures et Appliquées*, 157:101–135, 2022. URL: <https://www.sciencedirect.com/science/article/pii/S021782421001124>, doi:10.1016/j.matpur.2021.07.009.

[39] Jonathan W. Siegel and Jinchao Xu. High-order approximation rates for shallow neural networks with cosine and  $\text{ReLU}^k$  activation functions. *Applied and Computational Harmonic Analysis*, 58:1–26, 2022. URL: <https://www.sciencedirect.com/science/article/pii/S1063520321001056>, doi:10.1016/j.acha.2021.12.005.

[40] Luca Venturi, Afonso S. Bandeira, and Joan Bruna. Spurious valleys in one-hidden-layer neural network optimization landscapes. *Journal of Machine Learning Research*, 20(133):1–34, 2019. URL: <http://jmlr.org/papers/v20/18-674.html>.

[41] Qianchao Wang, Shijun Zhang, Dong Zeng, Zhaoheng Xie, Hengtao Guo, Tieyong Zeng, and Feng-Lei Fan. Don’t fear peculiar activation functions: EUAF and beyond. *Neural Networks*, 186:107258, 2025. URL: <https://www.sciencedirect.com/science/article/pii/S0893608025001376>, doi:10.1016/j.neunet.2025.107258.

[42] Rui Wang, Yuesheng Xu, and Mingsong Yan. Hypothesis spaces for deep learning. *Neural Networks*, 193 (2026), 107995, 14 pages. URL: <https://doi.org/10.1016/j.neunet.2025.107995>.

[43] Yuesheng Xu. Multi-grade deep learning. *Communications on Applied Mathematics and Computation*, 03 2025. doi:10.1007/s42967-024-00474-y.

[44] Yuesheng Xu. Successive affine learning for deep neural networks. *Analysis and Applications*, 23 (8) (2025), 1425–1467.

[45] Yuesheng Xu and Taishan Zeng. Multi-grade deep learning for partial differential equations with applications to the burgers equation. *arXiv preprint*, 2023. arXiv:2309.07401.

[46] Zhi-Qin John Xu, Yaoyu Zhang, Tao Luo, Yanyang Xiao, and Zheng Ma. Frequency principle: Fourier analysis sheds light on deep neural networks. *Communications in Computational Physics*, 28(5):1746–1767, 2020. URL: [http://global-sci.org/intro/article\\_detail/cicp/18395.html](http://global-sci.org/intro/article_detail/cicp/18395.html), doi:10.4208/cicp.0A-2020-0085.

[47] Zhi-Qin John Xu, Yaoyu Zhang, and Yanyang Xiao. Training behavior of deep neural network in frequency domain. In *Neural Information Processing: 26th International Conference, ICONIP 2019, Sydney, NSW, Australia, December 12–15, 2019, Proceedings, Part I* 26, pages 264–274. Springer, 2019.

[48] Dmitry Yarotsky. Error bounds for approximations with deep ReLU networks. *Neural Networks*, 94:103–114, 2017. URL: <http://www.sciencedirect.com/science/article/pii/S0893608017301545>, doi:10.1016/j.neunet.2017.07.002.

[49] Dmitry Yarotsky. Optimal approximation of continuous functions by very deep ReLU networks. In Sébastien Bubeck, Vianney Perchet, and Philippe Rigollet, editors, *Proceedings of the 31st Conference On Learning Theory*, volume 75 of *Proceedings of Machine Learning Research*, pages 639–649. PMLR, 06–09 Jul 2018. URL: <http://proceedings.mlr.press/v75/yarotsky18a.html>.

[50] Dmitry Yarotsky and Anton Zhevnerchuk. The phase diagram of approximation rates for deep neural networks. In H. Larochelle, M. Ranzato, R. Hadsell, M. F. Balcan, and H. Lin, editors, *Advances in Neural Information Processing Systems*, volume 33, pages 13005–13015. Curran Associates, Inc., 2020. URL: <https://proceedings.neurips.cc/paper/2020/file/979a3f14bae523dc5101c52120c535e9-Paper.pdf>.

[51] Shijun Zhang, Jianfeng Lu, and Hongkai Zhao. On enhancing expressive power via compositions of single fixed-size ReLU network. In Andreas Krause, Emma Brunskill, Kyunghyun Cho, Barbara Engelhardt, Sivan Sabato, and Jonathan Scarlett, editors, *Proceedings of the 40th International Conference on Machine Learning*, volume 202 of *Proceedings of Machine Learning Research*, pages 41452–41487. PMLR, 23–29 Jul 2023. URL: <https://proceedings.mlr.press/v202/zhang23ad.html>.

[52] Shijun Zhang, Jianfeng Lu, and Hongkai Zhao. Deep network approximation: Beyond ReLU to diverse activation functions. *Journal of Machine Learning Research*, 25(35):1–39, 2024. URL: <http://jmlr.org/papers/v25/23-0912.html>.

[53] Shijun Zhang, Hongkai Zhao, Yimin Zhong, and Haomin Zhou. Fourier multi-component and multi-layer neural networks: Unlocking high-frequency potential. *arXiv e-prints*, page arXiv:2502.18959, February 2025. [arXiv:2502.18959](https://arxiv.org/abs/2502.18959).

[54] Shijun Zhang, Hongkai Zhao, Yimin Zhong, and Haomin Zhou. Structured and balanced multicomponent and multilayer neural networks. *SIAM Journal on Scientific Computing*, 47(5):C1059–C1090, 2025. [arXiv:https://doi.org/10.1137/24M1675990](https://doi.org/10.1137/24M1675990), doi:10.1137/24M1675990.

[55] Shijun Zhang, Hongkai Zhao, Yimin Zhong, and Haomin Zhou. Why shallow networks struggle to approximate and learn high frequencies. *Information and Inference: A Journal of the IMA*, 14(3):iaaf022, 07 2025. [arXiv:https://academic.oup.com/imaiai/article-pdf/14/3/iaaf022/63829171/iaaf022.pdf](https://academic.oup.com/imaiai/article-pdf/14/3/iaaf022/63829171/iaaf022.pdf), doi:10.1093/imaiai/iaaf022.

[56] Ding-Xuan Zhou. Universality of deep convolutional neural networks. *Applied and Computational Harmonic Analysis*, 48(2):787–794, 2020. URL: <http://www.sciencedirect.com/science/article/pii/S1063520318302045>, doi:10.1016/j.acha.2019.06.004.